The gene *brain tumor* constrains growth to ensure proper patterning during regeneration in *Drosophila* imaginal discs

Short title: brain tumor and regenerative growth and patterning

Syeda Nayab Fatima Abidi[1] and Rachel K. Smith-Bolton[1,*]

[1] Department of Cell and Developmental Biology, University of Illinois Urbana-Champaign, Urbana, IL 61801, USA

* rsbolton@illinois.edu

Abstract

Regeneration after injury happens in a complex environment that requires precise orchestration of cell proliferation and establishment of correct patterning and cell-fate specification to ensure a fully functional outcome. Regenerative growth needs to be controlled and constrained to prevent overgrowth and to allow differentiation. However, the factors that are required to restrict regeneration to facilitate patterning of the regenerating tissue and establishment of correct cell fates have not been identified. Using a genetic ablation system in the *Drosophila* wing imaginal disc, we have identified the gene *brain tumor (brat)* as a protective factor that shields the regenerating tissue from excessive pro-growth gene activation and enables correct patterning and cell-fate specification. Regenerating discs with reduced levels of *brat* are unable to pattern correctly resulting in adult wings with a disrupted wing margin. This mis-patterning is due to elevated levels of the pro-growth factor Myc and the self-renewal factor Chinmo, which lead to suppression of the cell fate-specification gene *cut (ct)*. Thus, Brat protects regenerating tissue from erroneous patterning by constraining expression of pro-regeneration genes.

Introduction

Regeneration is the remarkable process by which some organisms replace tissues and organs after damage such that both morphology and function are restored. Complete regeneration requires several steps to occur correctly including wound healing, cell

proliferation, and proper patterning and cell-fate specification in the newly formed tissue. The degree of regenerative capacity varies among different species, ranging from whole-body regeneration in hydra and planaria to limited tissue regeneration in mammals. Work in several model organisms has identified signaling pathways and molecular mechanisms that are important for initiating and executing regenerative growth after tissue damage, including JNK signaling (1–5), JAK/STAT signaling (6–8), EGFR signaling (9–12), Hippo signaling (13–17), Wnt signaling (18–24), and Myc (23,25). Many of these mechanisms are also important during normal development, and the process of regeneration was traditionally thought to be a redeployment of earlier developmental steps (9,26–29). However, recent evidence suggests that regeneration is not a simple reiteration of development but can employ regeneration-specific regulatory mechanisms (3,25,30–34). Indeed, faithful regeneration likely requires additional mechanisms, since regrowth happens in the presence of wound-response signaling and in a developed juvenile or adult organism. Additionally, pro-growth pathways that are used during normal development are often activated in new ways and at higher strengths in the regenerating tissue (2,7,15,23). These augmented pro-growth signals must decline as regeneration progresses to prevent unrestrained growth and to enable re-establishment of pattern and cell-fate specification. Thus, regeneration-specific growth suppressors and additional patterning factors are likely used to terminate regeneration and allow differentiation (reviewed in 35). However, despite our understanding of the pro-growth signals needed for regeneration, we do not yet know what distinct regeneration-specific factors exist in different model organisms to restrain growth and promote re-patterning of regenerating tissue.

Drosophila melanogaster imaginal discs, precursors of adult fly appendages, are simple columnar epithelia that have well-characterized, complex expression of patterning genes that determine cell-fate specification. Imaginal discs undergo regeneration after damage (reviewed in 36), and we have previously used a genetic ablation system to study patterning in the regenerating tissue (23,32). Here we identify *brain tumor (brat)* as a critical growth regulator and patterning factor necessary for the establishment of proper cell fates during regeneration in *Drosophila* imaginal discs. Brat is a member of the TRIM- (tripartite motif containing)-NHL (NCL-1, HT2A, and LIN-41) family of proteins and functions as a translational repressor by binding to its target RNAs either independently or in a complex with Pumilio and Nanos (37–39). It acts as a potent differentiation factor and tumor suppressor in neural and ovarian germline stem cell lineages (40–43). Human and mouse orthologs of Brat, TRIM3 and TRIM32 respectively, also possess tumor-suppressor activity in glioblastomas and are required for neuronal differentiation (44,45). Furthermore, TRIM32 regulates muscle stem cell differentiation, which impacts muscular growth during development and regeneration (46,47). However, to our knowledge, TRIM-NHL family members have not been reported to have a function in regeneration that does not employ stem cells.

We show that regenerating wing imaginal discs with reduced levels of Brat regenerate better than controls, but the resulting adult wings have a disrupted margin. The margin loses some of the characteristic sensory bristles and veins, demonstrating an error in

cell-fate specification. Importantly, these phenotypes are regeneration-specific, as they are not observed in the mutant animals after normal development. The enhanced regeneration is due to increased expression of the growth regulators Myc and Wingless as well as upregulation of *ilp8,* which delays metamorphosis and allows the damaged tissue more time to regenerate. Intriguingly, the aberrant cell-fate specification is caused by elevated Myc expression, which is required for regenerative growth (23) but negatively regulates margin cell fates, likely through misregulation of the transcription factor Chronologically inappropriate morphogenesis (Chinmo), which inhibits differentiation. Hence, Brat acts as an important growth regulator and protective factor by constraining Myc and Chinmo levels during regeneration to prevent errors in patterning, cell-fate specification, and differentiation in the regenerating tissue. Because Brat's role in regeneration is reminiscent of its function in stem cell differentiation, we propose a general role for Brat as a key differentiation factor in different biological contexts.

Results

Brat suppresses regenerative growth and is required for wing margin cell-fate specification during regeneration

To identify genes important for regenerative growth and re-patterning, we performed a candidate screen, using our wing imaginal disc ablation system (23). The primordial wing was targeted for ablation at the early third-instar larval stage by using *rotund-GAL4* to drive the expression of the proapoptotic gene *reaper* for 24 hours (Fig 1A). Our ability

to restrict damage to 24 hours was provided by *tubulin-GAL80^{ts}*, which can inhibit GAL4 activity at 18°C, but allows GAL4-driven cell death at 30°C in the 24-hour window. The extent of wing imaginal disc regeneration in the larvae was reflected in the adult wing size. Hence, the resulting adult wings were scored based on size and patterning features to identify mutants that affect genes that are involved in regulating regenerative growth and establishment of cell fates. There is inherent variability in this system because of its sensitivity to environmental conditions such as temperature, humidity, and food quality, causing the results of different experiments to vary slightly (14,48–51). Animals with the same genotype within an experiment also showed some variation, due to stochastic differences in the time each animal takes to eclose, with animals that take longer to eclose having larger wings (23,50). However, differences between control and mutant animals using this system are reproducible, consistent, and have identified key regeneration genes (32,49–51).

Using this genetic ablation system, we identified the gene *brain tumor (brat)* as an important regulator of regenerative growth. *brat^{1}*/+ mutants that did not experience damage during development had adult wings that were not significantly different in size from controls (Fig S1A). However, after ablation and regeneration were induced, *brat^{1}*/+ mutants showed enhanced regeneration and had adult wings that were, on average, much larger than controls that had also undergone regeneration (Fig 1B and 1C). We confirmed this enhanced regeneration phenotype in heterozygotes for three other *brat* mutant alleles: *brat^{192}*, *brat^{150}* (52) and *brat^{11}* (53), as well as two deficiencies that remove the *brat* locus: *Df(2L)Exel8040* (54) and *Df(2L)TE37-7* (55) (Fig S1B and S1C).

113 The phenotype was weaker in the deficiencies, which affected multiple other genes in
114 addition to the *brat* locus, the reduction of which may ameliorate the *brat* mutant
115 phenotype.

116

117 Interestingly, we also discovered a role for *brat* in cell-fate specification during
118 regeneration. After normal development, $brat^{1}$/+ mutants had adult wings that were
119 patterned normally (Fig 1D, 1E and Fig S1D). To confirm that loss of *brat* does not
120 cause patterning errors during normal development, we knocked down Brat levels in the
121 entire wing pouch using *brat* RNAi, which resulted in adult wings that were patterned
122 normally (Fig S1E and S1F). A previous study in which Brat levels were reduced in the
123 anterior and posterior compartments of the wing also did not report any patterning
124 defects (56). However, when discs were ablated and allowed to regenerate, *brat*
125 heterozygous mutant wings showed aberrant patterning such that the wing margin lost
126 sensory bristles and vein material (Fig 1F and 1G). By contrast, control regenerated
127 wings lost margin tissue at a lower frequency (Fig 1H and 1I). Furthermore, the extent of
128 margin tissue lost was not as severe in control regenerated wings as compared to
129 $brat^{1}$/+ regenerated wings (Fig 1H and 1I). Similar to the enhanced regeneration seen in
130 *brat* mutants, we confirmed the loss-of-margin defect in heterozygotes for the additional
131 three mutant alleles and two deficiencies (Fig S1G and S1H). The deficiencies again
132 showed a weaker phenotype.

133

Brat often forms a complex with Pumilio to suppress its target mRNAs (37–39). However, we found that mutations in *pumilio* were unable to recapitulate the *brat* phenotype (Fig S1I). These data suggest a requirement for *brat,* independent of *pumilio,* in suppressing growth during regeneration and establishing correct cell fates at the wing margin.

brat **regulates entry into metamorphosis**

Tissue damage in imaginal discs can induce a systemic response in the larvae, which extends the larval phase of development and delays pupariation (23,57). This delay in pupariation is due to expression of the relaxin-like peptide *ilp8* in damaged discs (58,59). To determine whether *brat* mutants regenerated better due to an enhanced delay in pupariation, we measured rates of pupariation in control and mutant animals. We found that during normal development, control and $brat^{1}$/+ animals pupariated at the same time, indicating that the two genotypes develop at similar rates (Fig S2A). After disc damage, *brat* mutants delayed pupariation an additional day compared to controls in which discs were also damaged (Fig 2A and Fig S2B). The deficiencies also showed an enhanced delay, but it was not as pronounced as the delay experienced by the mutant alleles (Fig S2C), likely due to the deficiencies affecting multiple genes. Note that direct comparisons cannot be made between regenerating larvae that spent 24 hours at 30°C (Fig 2A, S2B and S2C) and normally developing larvae that remain at 18°C (Fig S2A), due to the effects of temperature on development. Our data show that *brat*/+ mutants are able to stay in the larval stage even longer than controls, giving them

more time to regenerate. The shorter delay in pupariation experienced by the deficiencies may account for their slightly decreased regenerative potential compared to *brat*^{1}/+ animals (Fig S1C).

To determine why discs with reduced Brat had an increased delay in pupariation, we measured *ilp8* transcript levels through qPCR. Undamaged control animals express very low *ilp8* levels. However, after regeneration was induced, we saw an 80-fold increase in *ilp8* levels in controls, while the *brat*^{1}/+ animals showed a 140-fold increase (Fig 2B). Thus, *brat* suppresses *ilp8* during regeneration, regulating the timing of pupariation.

brat **restricts growth and proliferation during regeneration**

Regenerative growth occurs through localized cell proliferation at the wound site (23,60).The proliferating cells, known as the blastema, give rise to the regenerated tissue. The blastema and the subsequent regenerated wing pouch can be labeled with the wing primordium marker Nubbin (Nub) (61). To determine whether *brat*^{1}/+ discs regenerated better due to increased growth rates in the wing pouch, we measured the area of the Nub-expressing cells in control and *brat*^{1}/+ regenerating discs. In the initial stages of regeneration, the control and mutant had similar Nub-expressing areas, indicating equal ablation and equal early regrowth. However, by 48 hours after tissue damage (recovery time 48, or R48), *brat*^{1}/+ wing discs had a significantly bigger Nub-expressing pouch than the control (Fig 2D, 2E and 2F), indicating that *brat*/+ mutants

were regenerating faster than controls. To assess whether this difference in growth rates was due to differences in proliferation, we counted cells going through mitosis by quantifying Phospho-histone H3 (PH3)-positive nuclei in the regenerating blastema. Reduction of *brat* resulted in a significantly higher number of PH3-positive nuclei per area at R0, but this increased proliferation had subsided to normal levels by R24 (Fig 2G, 2H and 2I). Differences in proliferation early in regeneration often become evident later when measuring wing pouch area (51). Therefore, reduction of *brat* gives the regenerating tissue a growth advantage early in regeneration, resulting in a measurable difference in tissue area by R48.

Wingless (Wg) and Myc are regulators of regenerative growth and are upregulated at the wound site after damage (20,21,23). Interestingly, Brat regulates stem cell differentiation in the brain by suppressing self-renewal factors such as Wnt signaling and Myc to enable specification of progenitor cell fate (42,62). Additionally, Brat overexpression can suppress Myc levels in wing disc epithelial cells, although loss of *brat* does not lead to elevated Myc levels in wing discs during normal development (56). To determine whether these regulators of regenerative growth are upregulated in $brat^{1}$/+ regenerating discs, we examined the expression of Wg and Myc. Wg is normally expressed along the Dorso-ventral (DV) boundary and in two concentric circles at the inner and outer edge of the wing pouch (63, Fig 3A), and Myc is expressed in the wing pouch, but is repressed in the cells at the DV boundary as they undergo cell cycle and growth arrest (64, Fig 3B). Both Wg and Myc expression were comparable to controls in undamaged $brat^{1}$/+ discs (Fig S3A, S3B, S3C, S3D and S3E). When damage is

induced, Wg is upregulated throughout the blastema by R0 (23, Fig 3C). Reduction of *brat* expression resulted in significantly higher levels of Wg expression at R0 (Fig 3D and 3E) but not at R24 (Fig 3F). After ablation, Myc expression is elevated in the regenerating tissue (23, Fig 3G and 3H). $brat^{1}$/+ discs showed significantly higher levels of Myc at R0, which were sustained through R24 (Fig 3I, 3J and 3K). Thus, loss of *brat* caused an increase in the levels of both Wg and Myc early in regeneration. The elevated expression of these growth regulators likely explains the high proliferation seen in $brat^{1}$/+ discs at R0, and the larger wing pouch at R48.

brat **is required for margin cell-fate specification during regeneration**

Reduction of *brat* during regeneration caused patterning defects specifically at the wing margin, resulting in the loss of vein at the margin and loss of sensory bristles (Fig 1G). Thus, *brat* is required for correct cell-fate specification at the DV boundary during regeneration. The wing imaginal disc is divided into the dorsal and the ventral compartments, with expression of the LIM-homeodomain protein Apterous (Ap) in dorsal cells. The juxtaposition of the dorsal and ventral cells forms the DV boundary, which develops into the adult wing margin (65, Fig 4A). Notch (N) and Wg signaling at the DV boundary are crucial for the correct organization and cell-fate specification at the boundary (66). *cut (ct)* and *achaete (ac)* are margin-specific genes that are expressed downstream of N and Wg signaling. *ct* is required for the specification of the wing margin, and *ac* specifies the pro-neural sensory organ precursors (66,67, Fig 4A).

To investigate whether the errors in fate specification seen in *brat*^{1}/+ discs were due to a compromised compartment boundary, we examined the expression of Ap using the *ap-lacZ* reporter. *ap-lacZ* expression showed a clear DV boundary in the undamaged control discs (Fig 4B). The DV boundary remained intact after ablation in control and *brat*^{1}/+ discs (Fig 4C, 4D, Fig S4A and S4B). *ap-lacZ* expression was also seen in the debris found in the damaged wing imaginal disc, due to the perdurance of β-gal. Furthermore, Wg expression was restored to its normal DV expression by R48 in both control and *brat*^{1}/+ discs (Fig S4C and S4D). Therefore, the patterning defects were not caused by disruptions in the DV boundary or changes in Wg expression.

Next, we examined N signaling in *brat*^{1}/+ discs due to its critical role in specifying fates at the DV boundary. We used a N signaling reporter, which uses *Notch Response Elements* (*NREs*) that bind to the Notch co-receptor Suppressor of Hairless, to drive the expression of GFP (68). No difference was detected in the expression of the N reporter for undamaged control and *brat*^{1}/+ discs (Fig 4E and 4F). N signaling at the DV boundary was restored by R24 in controls and continued at R48 (Fig 4G and 4H). Note that the reporter signal can also be seen in cellular debris in the regenerating discs due to the perdurance of GFP. Interestingly, *brat*^{1}/+ discs showed highly elevated levels of the N signaling reporter at both these time points (Fig 4I and 4J). This result is consistent with recent evidence demonstrating Brat's ability to attenuate N nuclear transport in the brain (69).

Brat does not regulate margin cell-fate specification through Notch signaling

While loss of the wing margin is normally associated with reduced N signaling, we wondered whether this elevated N signaling could also disrupt margin fates. Indeed, a screen for N regulators found that up-regulation of N signaling in the wing disc could also result in notches (68). However, we have shown that in regenerating discs, elevated N signaling cannot replicate the $brat^{1}$/+ phenotype, and reducing N signaling in the $brat^{1}$/+ mutant does not rescue the patterning defect. To test whether increasing N signaling could phenocopy the *brat* mutation, we overexpressed the N-intracellular domain in the wing pouch during the 24-hour ablation period (Fig S4E and S4F). Regenerating discs that experienced increased N activity in the wing pouch resulted in adult wings that were patterned remarkably well, with significantly fewer wings showing any margin defects when compared to the control (Fig S4G). Thus, increased N activity during regeneration suppresses margin defects.

To assess whether decreasing N activity in $brat^{1}$/+ regenerating discs could rescue the margin defect phenotype. We used a mutation in the *anterior pharynx defective 1 (aph-1)* gene to downregulate N signaling. *aph-1* is part of an enzyme complex that is involved in the proteolytic cleavage of the N transmembrane protein, which allows the N intracellular domain to translocate into the nucleus to activate its target genes (reviewed in 70). Undamaged $aph\text{-}1^{D35}$/+ discs showed significantly reduced N signaling (Fig S4H, S4I and S4J). N signaling was also reduced in regenerating $aph\text{-}1^{D35}$/+ discs at R24 (Fig S4K, S4L and S4M). Regenerating $aph\text{-}1^{D35}$/+ discs resulted in adult wings that showed

a frequency of margin defects very similar to *brat*^{1}/+ (Fig S4N), consistent with reduced N activity causing wing margin errors. Importantly, the *aph-1*^{D35} mutant was unable to rescue the loss of *brat* margin phenotype (Fig S4N). Thus, while Brat constrains N signaling during regeneration, the elevated N signaling in *brat*^{1}/+ mutants does not cause the margin cell-fate specification defects.

brat specifies margin fate by controlling the expression of Cut and Achaete

To understand how patterning was disrupted in *brat*^{1}/+ regenerating discs, we examined expression of margin cell-fate genes. Cut (Ct) expression was present along the DV boundary in both undamaged control and *brat*^{1}/+ discs (Fig 4K and 4L), consistent with our results showing that adult undamaged *brat*^{1}/+ wings do not have margin defects (Fig S1D). In control regenerating discs, Ct expression was detected at the DV boundary at R72, which is when regeneration and repatterning are largely complete (Fig 4M). By contrast, Ct expression was either not observed in *brat*^{1}/+ discs or was still missing in segments of the DV boundary at R72 (Fig 4N and 4O). These results indicate a specific error in cell-fate specification, as the DV boundary was intact at R72 (Fig S4A and S4B). Undamaged control and *brat*^{1}/+ discs also showed appropriate Ac expression in two stripes of cell directly flanking the DV boundary in the anterior half of the disc (Fig 4P and 4Q). Ac expression was also detected in control regenerating discs at R72 (Fig 4R). While Ac-expressing cells appeared in *brat*^{1}/+ discs, they were not clearly separated across the DV boundary (Fig 4S). This finding is consistent with previous reports showing that Ct suppresses Ac at the margin, and mutations in *ct* lead to aberrant

289 expression of Ac at the DV boundary, followed by degeneration of the wing margin
290 through cell death (71,72).

291

292 **High Myc expression perturbs margin cell-fate specification during regeneration**

293 Our results show that Brat both restricts regenerative growth and ensures correct cell-
294 fate specification at the wing margin. Interestingly, JNK signaling in regenerating tissue
295 can cause aberrant posterior-to-anterior cell-fate changes, which can be suppressed by
296 a regeneration-specific protective factor, Taranis, to ensure correct patterning of the
297 regenerating tissue (32). Therefore, we wondered whether unconstrained regenerative
298 growth, or unconstrained expression of growth drivers, could also have deleterious side
299 effects such as loss of margin cell fates. As Wg expression is normal during late
300 regeneration and we have ruled out elevated N signaling as the causative factor for the
301 cell-fate errors that occurred in $brat^{1}$/+ regenerating discs, we wondered whether high
302 Myc expression could cause the margin defects.

303

304 Brat overexpression can suppress Myc in wing imaginal disc cells (56), and in
305 undamaged wing discs Brat protein levels were elevated at the DV boundary where Myc
306 was reduced (Fig 5A-A''), suggesting that Brat may regulate Myc at the DV boundary.
307 To test whether high Myc levels could cause margin defects during regeneration and
308 phenocopy the *brat* mutation, we overexpressed Myc in the wing pouch during the 24-
309 hour ablation period. Myc was highly upregulated at R0 (Fig 5B, 5C and 5D), but Myc
310 levels had returned to normal by R24 (Fig 5D). Overexpression of Myc also resulted in a

311 significantly higher number of proliferating nuclei in the regenerating tissue at R0,
312 similar to *brat*^{1}/+ discs (Fig 5E, 5F and 5G). Remarkably, we observed that adult wings
313 resulting from Myc-overexpressing regenerating discs also showed margin defects
314 similar to the *brat*^{1}/+ wings (Fig 5H and 5I). Moreover, the frequency of margin defects
315 in the adult wings resulting from Myc-overexpressing regenerating discs was even
316 higher than in adult wings resulting from *brat*^{1}/+ regenerating discs (Fig 5J),
317 demonstrating that elevated levels of Myc alone can cause errors in margin cell-fate
318 specification. Overexpressing Myc for a 24-hour window during normal development
319 resulted in 3 adult wings out of 730 that showed any margin defects (Fig S5A). Even in
320 these wings, only one segment of the margin was affected. These data indicate that
321 high Myc levels do not cause cell-fate specification errors during normal development,
322 and the extensive loss of wing margin induced by high Myc expression is a
323 regeneration-specific phenotype. Similar to *brat*^{1}/+ discs, *ap-lacZ* expression showed
324 that the compartment boundary was not compromised in Myc-overexpressing
325 regenerating discs (Fig 5K and 5L). Likewise, Ct expression was missing in segments at
326 the DV boundary as in the *brat*^{1}/+ discs (Fig 5M and 5N).

327

328 We hypothesized that if the *brat* phenotype was due to elevated Myc levels, we would
329 be able to rescue the phenotype by reducing Myc levels in the *brat* mutant. For this
330 purpose, we used *dm*^{4}, which is a null allele of Myc (73). Surprisingly, we observed that
331 the *dm*^{4}/+ mutants alone showed margin defects in the regenerated wings at a
332 frequency similar to *brat*^{1}/+, even though the *dm*^{4}/+; *brat*^{1}/+ double mutant showed
333 slightly reduced frequency of margin defects (Fig S5B). To confirm that Myc levels were

reduced in the *dm*^{4}/+ mutants, we quantified Myc protein through immunostaining. We observed that there was no significant difference in Myc expression levels between the *dm*^{4}/+ mutant and control, both during development and regeneration (Fig S5C and S5D). Indeed, Myc levels were trending higher in the *dm*^{4}/+ discs during regeneration. The failure of the *dm*^{4} mutation to reduce Myc levels could be due to compensatory expression of the functional copy of the Myc locus. We next tried reducing Myc levels though RNAi. Despite the RNAi expression being transient in our system, and only occurring in cells that survive ablation, RNAi-mediated persistent knockdown has worked for multiple genes, likely due to the shadow RNAi effect (74). Two RNAi lines could significantly reduce Myc levels during normal development when expressed during early third instar (Fig S5E). However, when Myc RNAi was expressed during the 24-hour ablation period, Myc levels were not reduced at either R0 or R24, with one Myc RNAi line showing significantly higher levels of Myc compared to the control (Fig S5F). Thus, compensatory regulation of Myc expression during regeneration prevented us from testing whether reduction in Myc could rescue the *brat*/+ phenotype.

Interestingly, animals that overexpressed Myc in the wing pouch during ablation did not undergo a regeneration-induced pupariation delay (Fig S5G), suggesting that Brat regulates the entry into metamorphosis independently of its regulation of Myc. Therefore, not all loss of Brat effects are mediated through Myc.

Driving growth in multiple ways can disrupt patterning during regeneration

Myc is an important driver of regenerative growth, and yet, we found that cell-fate specification during regeneration can be negatively affected if Myc levels are left unchecked. To test whether the aberrant patterning was a specific result of high Myc levels or whether increases in growth and proliferation could, in general, cause margin defects, we sought to overexpress other growth drivers such as *yorkie (yki)* and *string (stg)*.

Overexpressing *yki* and *stg* in the wing imaginal disc during the 24-hour ablation period caused the resulting adult wings to be much larger than controls that had also undergone damage and regeneration (Fig 6A), indicating that *yki* and *stg* are both able to drive regenerative growth. In both of these cases, no regeneration-induced pupariation delay was seen, making the enhanced regeneration even more remarkable (Fig 6B). Intriguingly, we observed loss of margin tissue after *yki* overexpression during regeneration similar to $brat^{1}$/+ wings (Fig 6C, 6D and 6F) but did not observe many margin defects for wings that had experienced *stg* overexpression during regeneration. By contrast, overexpression of *stg* produced various patterning errors within the wing blade, different from the defects seen in $brat^{1}$/+ wings (Fig 6E and 6F). Similar to both regenerating $brat^{1}$/+ and Myc-overexpressing discs, *yki* overexpression during ablation led to loss of Ct expression at the DV boundary (Fig 6G and 6H), explaining the adult phenotype. Importantly, *yki* overexpression led to increased Myc expression in R24 discs (Fig 6I, 6J and 6K), suggesting that ectopically increased Yki levels likely suppressed margin cell-fate specification by inducing Myc overexpression. Thus, overexpression of pro-growth factors can disrupt patterning in regenerating tissue in a

379 variety of ways. However, since overexpression of *stg* did not cause loss of margin, this
380 phenotype is not caused by enhancing growth in general.

381

382 **Loss of cell-fate specification may be due to elevated expression of Chinmo**

383 Given that driving growth by overexpressing String does not cause loss of wing margin
384 cell fates in regenerating tissue, this phenotype might not be caused by increased
385 growth overall but by misregulation of one or more targets of the Myc transcription
386 factor. We have previously identified the gene *Chronologically inappropriate*
387 *morphogenesis (chinmo)* as a novel regulator of regeneration (50). Chinmo is a
388 transcription factor that regulates the balance between a proliferative self-renewal state
389 and a differentiated state in stem cells (75,76). Recent work has shown that *chinmo* also
390 maintains wing epithelial cells in an unspecified state during development by inhibiting
391 *ct* expression, and enhances regenerative potential (77). While *chinmo* mRNA is a
392 direct Brat target (39), *chinmo* is regulated at the level of transcription in the wing
393 imaginal disc (77). Therefore, we wondered whether *chinmo* could be misregulated
394 downstream of Myc in the $brat^{1}$/+ regenerating discs, leading to inhibition of Ct
395 expression. Interestingly, the model organism Encyclopedia of Regulatory Networks
396 (modERN) data show Myc binding near the *chinmo* promoter, supporting this
397 hypothesis (78). Chinmo levels were not significantly different in undamaged control and
398 $brat^{1}$/+ discs (Fig 7A, 7B and 7E). However, Chinmo levels were significantly higher in
399 $brat^{1}$/+ regenerating discs compared to control regenerating discs at R24 (Fig 7C, 7D

and 7F). Thus, the loss of *ct* expression and loss of margin cell fates in *brat/+* regenerating discs are likely due, at least in part, to upregulation of *chinmo*.

To confirm regulation of *chinmo* downstream of Myc, we examined Chinmo levels in regenerating discs over-expressing Myc. Chinmo levels were elevated in Myc-overexpressing discs at R0, when Myc overexpression was the highest (Fig 5D and Fig 7G-I). However, Chinmo levels were restored to control levels by R24 in Myc-overexpressing discs, consistent with the return of Myc levels to normal at this time point (Fig 5D and Fig S6A-C). Interestingly, Myc and Chinmo expression almost perfectly co-localized, consistent with the hypothesis that Myc regulates Chinmo expression (Fig S6A-B''). Additionally, we observed a high correlation between Myc and Chinmo expression levels in individual discs (Fig S6D-E). While Myc likely regulates Chinmo, the increase in Chinmo levels at R0 may not be the only contributing factor towards *ct* misregulation in Myc-overexpressing regenerating discs, and other Myc targets may also be involved.

Based on our findings, we propose a model in which pro-growth factors are important for coordinating regenerative growth, but can lead to deleterious side effects by perturbing cell-fate gene expression and patterning. Brat prevents a prolonged proliferative and unspecified state in regenerating wing discs by inhibiting Wg, Ilp8, Myc and Chinmo to enable cessation of growth, induction of cell-fate specification, and entry into metamorphosis (Fig 8).

Discussion

Here we have shown that Brat acts as a protective factor during regeneration by constraining levels of transcription factors such as Myc and Chinmo, which promote growth and proliferation but also inhibit cell-fate specification. If Brat is unable to perform its protective function during regeneration, Myc levels increase unchecked, resulting in misregulation of its targets, including Chinmo and subsequently Ct, causing loss of proper cell fates at the wing margin. In addition, we have demonstrated that overexpression of Yki and Stg can both result in different types of patterning defects, indicating that growth regulators must be tightly controlled during regeneration to ensure correct establishment of cell fates.

Myc is broadly used across organisms to promote proliferation and prevent differentiation (79,80), and Myc is strongly activated in the regenerating tissue and is required for efficient regeneration. Importantly, increased Myc levels can enhance regeneration in both younger discs as well as mature discs that normally regenerate poorly (23,25). Nevertheless, we have found that while these abnormally high Myc levels can enhance regenerative growth, they also perturb differentiation by misregulating target genes such as Chinmo. Thus, enhanced regeneration happens at the expense of correct cell-fate specification, and the regenerating tissue must employ mechanisms to suppress high regeneration signaling.

Brat promotes differentiation in *Drosophila* larval neuroblasts and ovarian germline stem cells by asymmetrically segregating to one of the daughter cells where it post-transcriptionally inhibits Myc (41,42). This daughter cell is then able to differentiate while the other daughter cell remains a stem cell. In *brat* mutants, progeny of stem cells are unable to differentiate, resulting in an abnormal expansion of the stem-cell population, which can form tumors in the brain (40–43). Thus, Brat protects these tissues from overproliferation of stem cells. Importantly, wing imaginal disc regeneration is not stem-cell based, but in wing disc regeneration Brat also inhibits Myc to prevent excessive proliferation and allow correct cell-fate specification. Based on these similarities in function, Brat likely acts as a protective factor across different biological contexts, including regeneration that does not employ stem cells.

We have previously shown that JNK signaling can induce posterior-to-anterior fate changes in regenerating wing discs, which can be prevented by the protective factor Taranis (31). We have now identified a second protective factor, Brat, which is needed specifically for correct patterning of the regenerating wing margin. Interestingly, while elevated JNK signaling causes anterior markers to appear in the posterior wing compartment, it does not cause margin loss, indicating that posterior fate and margin fate are regulated in distinct ways (32). Protective factors such as Tara and Brat are important for maintaining the balance between fate specification and pluripotency, but they do so by using very different mechanisms. While the molecular function of Tara is unknown, genetic interactions in *Drosophila* coupled with the demonstrated functions of its vertebrate homologs suggest it regulates gene expression at the level of transcription

and chromatin (81–84). By contrast, Brat acts as a translational repressor, and suppresses its targets through mRNA degradation (85,86). Tara is required to prevent fate changes induced by JNK signaling, which is necessary for wound repair and regeneration but is not required for the normal development of the wing. By contrast, Myc is required for both development and regeneration of the wing disc, but is constrained by Brat only during regeneration.

An important open question in the field of regeneration is how patterning and cell-fate specification are regulated in regenerating tissue, and whether these mechanisms are different from the developmental program. Many studies have highlighted that regeneration must be distinct from development in some ways, because the damaged tissue is already complexly patterned, and the wound-healing response causes strong activation of signaling pathways, some of which are not normally present in developing tissue (1,3,25,30–35). We are just beginning to identify regulators like Brat that are critical for attenuating regenerative growth signaling and shielding the regenerating tissue from the harmful side effects of such signaling. Identification of these regulators highlights the fact that the regenerating tissue behaves distinctly from normally developing tissue. Since regeneration signaling is complex and comprises many signaling pathways, many additional factors that play protective roles during regeneration likely exist. Identification of these additional factors will be important for the development of more useful clinical therapies targeted at tissue repair, which currently focus on replicating development without accounting for the deleterious side effects of exogenous and unconstrained pro-growth signaling.

Materials and Methods

Ablation and Regeneration experiments

Ablation experiments were done as previously described (32). Briefly, cell death was induced by driving *UAS-reaper* under *rotund-GAL4*, with $GAL80^{ts}$ for temporal control. Animals were raised at 18°C for 7 days after egg lay (AEL) (early third instar) before they were shifted to a 30°C circulating water bath for 24 hours. Animals were brought back to 18°C to allow regeneration. Wing discs were dissected at different time points after the end of ablation, or the animals were allowed to grow to adulthood to observe the adult wing phenotype. Undamaged control wing discs were the same genotype as the experimental animals but kept at 18°C and dissected on day 9 after egg lay, which is mid-late third instar. For undamaged adult wings, the animals were kept at 18°C until after eclosion. Any other undamaged conditions used are mentioned specifically in the figure legends.

Fly stocks

The following *Drosophila* stocks were used: w^{1118} (wild type)(87), w^{1118} *; rnGAL4, UAS-rpr, tubGAL80ts/TM6B,tubGAL80* (23), $brat^{1}$ (88)(FBst0003988), $brat^{192}$ and $brat^{150}$ (52)(a gift from Juergen Knoblich, Austrain Academy of Science), $brat^{11}$ (53)(a gift from Chen-Yu Lee, University of Michigan), *Df(2L)Exel8040* (54)(FBst0007847), *Df(2L)TE37C-7* (55)(FBst0006089), *rnGAL4, tubGAL80ts/TM6B* (23),

P{Trip.HM05078}attP2 (called *bratRNAi* in the text)(FBst0028590), *P{CaryP}attP2* (called *attP2* control in the text)(FBst0036303), *{PZ}ap^{rK568}* (89)(FBst0005374), *NRE-GFP* (68)(FBst0030727), *UAS-Nintra* (a gift from Gary Struhl, Columbia University), *aph-1^{D35}* (90)(FBst0063242), *UAS-Myc* (91)(FBst0009674), *UAS-yki* (92)(FBst0028836), *UAS-stg* (FBst0004778), *dm^{4}* (73), *P{GD1419}v2947* (called *MycRNAi#1* in the text)(VDRC ID# 2947) and *P{GD1419}v2948* (called *MycRNAi#2* in the text)(VDRC ID# 2948), *P{GD6000}v15293* (called control in the text) (VDRC ID# 15293)(93). All fly stocks are available from the Bloomington Drosophila Stock Center unless stated otherwise.

Pupariation timing

Pupariation experiments were performed in a similar manner to the ablation experiments. Starting at day 9, newly formed pupal cases were counted in each vial. Pupal cases were counted every 24 hours, up until day 15. Pupariation rates from three independent experiments were used to calculate the average plotted in the graphs.

Immunohistochemistry

Immunostaining was carried out as previously described (23). Primary antibodies were rat anti-Brat (1:200) (37) (a gift from Robin Wharton, Ohio State University), mouse anti-Nubbin (1:500) (94) (a gift from Steve Cohen, University of Copenhagen), rabbit anti-Phospho-Histone H3 (1:500) (Millipore), mouse anti-Wingless (1:100) (The Developmental Studies Hybridoma Bank [DSHB]), rabbit anti-dMyc (1:500) (Santa Cruz

Biotechnologies), mouse anti-βgal (1:100) (DSHB), mouse anti-Cut (1:10) (DSHB), mouse anti-Achaete (1:10)(DSHB), rat anti-Chinmo (1:500) (a gift from Nick Sokol, Indiana University). The Developmental Studies Hybridoma Bank (DSHB) was created by the NICHD of the NIH and is maintained at the University of Iowa, Department of Biology, Iowa City, IA 52242.

Secondary antibodies were AlexaFluor probes (1:1000) (Life Technologies). DNA was marked using TO-PRO3 (1:500) (Life Technologies) or DAPI (1:5000 of 0.5 mg/mL stock) (Sigma). Discs were mounted in Vectashield mounting medium (Vector Laboratories).

Discs were imaged on a Zeiss LSM 510 or a Zeiss LSM 700 confocal microscope. Parameters for imaging were identical for quantified images. Images were processed using ZEN lite (Zeiss), ImageJ (NIH) and Photoshop (Adobe). Maximum intensity projections were created for the confocal images. Fluorescence intensity was measured within the wing pouch as marked by anti-Nubbin or by using the morphology of the undamaged wing disc. Myc and Chinmo intensities were measure by outlining the region expressing elevated Myc or Chinmo levels. *NRE-GFP* intensity was measured by outlining the GFP-expressing region at the DV boundary.

Adult wing quantifications

554 Adult wings were mounted in Gary's Magic Mount (Canada balsam [Sigma] dissolved in
555 methyl salicylate [Sigma]). Images were taken with an Olympus SZX10 microscope with
556 an Olympus DP21 camera using the CellSens Dimension software (Olympus).
557
558 All adult wings that were 75% or 100% the size of a normal wing were used to quantify
559 the loss of the wing margin. The wing margin was divided into five segments defined by
560 where the wing veins intersect the margin. Each wing was scored for the number of
561 segments with missing margin to assess the extent of the patterning defect.
562 Percentages from the three independent experiments were used to calculate averages
563 plotted in the graphs. The area of undamaged and regenerated wings was measured
564 using ImageJ (NIH). ImageJ was also used to measure the percentage of linear length
565 of margin lost for the entire perimeter of the wing. Graphs were plotted using Excel and
566 Graphpad Prism 7.
567
568

569 **qPCR**

570 For quantitative PCR (qPCR), 40-60 wing imaginal discs were collected in Schneider's
571 medium and stored at -80°C. RNA was extracted using the Qiagen RNeasy Mini Kit
572 (#74104), and cDNA synthesis was performed using the Superscript III First Strand
573 Synthesis kit (#11752-050). qPCR reactions using the Power SYBR Green MasterMix
574 (ABI) were run on the ABI Step One Plus Real Time PCR System. The experiment
575 consisted of 3 biological replicates. For each biological replicate there were three
576 technical replicates. Gene expression was analyzed by the $\Delta\Delta C_t$ method and

normalized to *Gapdh2* expression. The following primers were used: *Gapdh2* forward primer (GTGAAGCTGATCTCTTGGTACGAC), reverse primer (CCGCGCCCTAATCTTTAACTTTTAC) (95), and *ilp8* primers used from Qiagen (QT00510552).

Acknowledgements

The authors would like to thank Amanda Brock and Sumbul Khan for critical reading of the manuscript and helpful discussions; Juergen Knoblich, Chen-Yu Lee, Gary Struhl, Robin Wharton, Nick Sokol, the Bloomington Drosophila Stock Center (NIH P40OD018537), Vienna Drosophila Resource Center and the Developmental Studies Hybridoma Bank for reagents.

References

1. Bosch M, Serras F, Martín-Blanco E, Baguñà J. JNK signaling pathway required for wound healing in regenerating Drosophila wing imaginal discs. Dev Biol. 2005 Apr;280(1):73–86.

2. Bergantinos C, Corominas M, Serras F. Cell death-induced regeneration in wing imaginal discs requires JNK signalling. Development. 2010 Apr 1;137(7):1169–79.

3. Bosch M, Bishop S-A, Baguna J, Couso J-P. Leg regeneration in Drosophila abridges the normal developmental program. Int J Dev Biol. 2010;54(8-9):1241–50.

4. Tasaki J, Shibata N, Sakurai T, Agata K, Umesono Y. Role of c-Jun N-terminal

598 kinase activation in blastema formation during planarian regeneration: JNK activation in
599 planarian regeneration. Dev Growth Differ. 2011 Apr;53(3):389–400.

600 5. Martín R, Pinal N, Morata G. Distinct regenerative potential of trunk and
601 appendages of *Drosophila* mediated by JNK signalling. Development. 2017 Nov
602 1;144(21):3946–56.

603 6. Bando T, Ishimaru Y, Kida T, Hamada Y, Matsuoka Y, Nakamura T, et al.
604 Analysis of RNA-Seq data reveals involvement of JAK/STAT signalling during leg
605 regeneration in the cricket Gryllus bimaculatus. Development. 2013 Mar 1;140(5):959–
606 64.

607 7. Katsuyama T, Comoglio F, Seimiya M, Cabuy E, Paro R. During *Drosophila* disc
608 regeneration, JAK/STAT coordinates cell proliferation with Dilp8-mediated
609 developmental delay. Proc Natl Acad Sci. 2015 May 5;112(18):E2327–36.

610 8. Verghese S, Su TT. STAT, Wingless, and Nurf-38 determine the accuracy of
611 regeneration after radiation damage in Drosophila. Bosco G, editor. PLOS Genet. 2017
612 Oct 13;13(10):e1007055.

613 9. Nakamura T, Mito T, Bando T, Ohuchi H, Noji S. Molecular and Cellular Basis of
614 Regeneration and Tissue Repair: Dissecting insect leg regeneration through RNA
615 interference. Cell Mol Life Sci. 2008 Jan;65(1):64–72.

616 10. Jiang H, Grenley MO, Bravo M-J, Blumhagen RZ, Edgar BA. EGFR/Ras/MAPK
617 Signaling Mediates Adult Midgut Epithelial Homeostasis and Regeneration in
618 Drosophila. Cell Stem Cell. 2011 Jan;8(1):84–95.

11. Fan Y, Wang S, Hernandez J, Yenigun VB, Hertlein G, Fogarty CE, et al. Genetic Models of Apoptosis-Induced Proliferation Decipher Activation of JNK and Identify a Requirement of EGFR Signaling for Tissue Regenerative Responses in Drosophila. Perrimon N, editor. PLoS Genet. 2014 Jan 30;10(1):e1004131.

12. Jin Y, Ha N, Forés M, Xiang J, Gläßer C, Maldera J, et al. EGFR/Ras Signaling Controls Drosophila Intestinal Stem Cell Proliferation via Capicua-Regulated Genes. Clurman BE, editor. PLOS Genet. 2015 Dec 18;11(12):e1005634.

13. Bando T, Mito T, Maeda Y, Nakamura T, Ito F, Watanabe T, et al. Regulation of leg size and shape by the Dachsous/Fat signalling pathway during regeneration. Development. 2009 Jul 1;136(13):2235–45.

14. Sun G, Irvine KD. Regulation of Hippo signaling by Jun kinase signaling during compensatory cell proliferation and regeneration, and in neoplastic tumors. Dev Biol. 2011;350(1):139–51.

15. Grusche FA, Degoutin JL, Richardson HE, Harvey KF. The Salvador/Warts/Hippo pathway controls regenerative tissue growth in Drosophila melanogaster. Dev Biol. 2011 Feb;350(2):255–66.

16. Hayashi S, Ochi H, Ogino H, Kawasumi A, Kamei Y, Tamura K, et al. Transcriptional regulators in the Hippo signaling pathway control organ growth in Xenopus tadpole tail regeneration. Dev Biol. 2014 Dec;396(1):31–41.

17. Grijalva JL, Huizenga M, Mueller K, Rodriguez S, Brazzo J, Camargo F, et al. Dynamic alterations in Hippo signaling pathway and YAP activation during liver

regeneration. Am J Physiol-Gastrointest Liver Physiol. 2014 Jul 15;307(2):G196–204.

18. Hobmayer B. WNT signallingmolecules act in axis formation in the diploblastic metazoan Hydra. Nature. 2000;407(6801):186–9.

19. Kawakami Y, Rodriguez Esteban C, Raya M, Kawakami H, Marti M, Dubova I, et al. Wnt/beta-catenin signaling regulates vertebrate limb regeneration. Genes Dev. 2006 Dec 1;20(23):3232–7.

20. McClure KD, Schubiger G. A screen for genes that function in leg disc regeneration in Drosophila melanogaster. Mech Dev. 2008 Jan;125(1-2):67–80.

21. Schubiger M, Sustar A, Schubiger G. Regeneration and transdetermination: The role of wingless and its regulation. Dev Biol. 2010 Nov;347(2):315–24.

22. Wehner D, Cizelsky W, Vasudevaro MD, Özhan G, Haase C, Kagermeier-Schenk B, et al. Wnt/β-Catenin Signaling Defines Organizing Centers that Orchestrate Growth and Differentiation of the Regenerating Zebrafish Caudal Fin. Cell Rep. 2014 Feb;6(3):467–81.

23. Smith-Bolton RK, Worley MI, Kanda H, Hariharan IK. Regenerative Growth in Drosophila Imaginal Discs Is Regulated by Wingless and Myc. Dev Cell. 2009 Jun;16(6):797–809.

24. Hanovice NJ, Leach LL, Slater K, Gabriel AE, Romanovicz D, Shao E, et al. Regeneration of the zebrafish retinal pigment epithelium after widespread genetic ablation. Barsh GS, editor. PLOS Genet. 2019 Jan 29;15(1):e1007939.

25. Harris RE. Localized epigenetic silencing of a damage-activated WNT enhancer

661 limits regeneration in mature Drosophila imaginal discs. Elife. 2016;3(5).

662 26. Muneoka K. Evidence that patterning mechanisms in developing and
663 regenerating limbs are the same. Nature. 298(5872):369–71.

664 27. Gupta V, Gemberling M, Karra R, Rosenfeld GE, Evans T, Poss KD. An Injury-
665 Responsive Gata4 Program Shapes the Zebrafish Cardiac Ventricle. Curr Biol. 2013
666 Jul;23(13):1221–7.

667 28. Roensch K. Progressive Specification Rather than Intercalation of Segments
668 During Limb Regeneration. Science. 2013;342(6164):1375–9.

669 29. Mader MM. Photoreceptor Differentiation during Retinal Development, Growth,
670 and Regeneration in a Metamorphic Vertebrate. J Neurosci. 2004 Dec
671 15;24(50):11463–72.

672 30. McCusker CD, Gardiner DM. Positional Information Is Reprogrammed in
673 Blastema Cells of the Regenerating Limb of the Axolotl (Ambystoma mexicanum).
674 Tsonis PA, editor. PLoS ONE. 2013 Sep 27;8(9):e77064.

675 31. Myohara M. Differential tissue development during embryogenesis and
676 regeneration in an annelid. Dev Dyn. 2004 Oct;231(2):349–58.

677 32. Schuster KJ, Smith-Bolton RK. Taranis Protects Regenerating Tissue from Fate
678 Changes Induced by the Wound Response in Drosophila. Dev Cell. 2015 Jul;34(1):119–
679 28.

680 33. Luttrell SM, Gotting K, Ross E, Alvarado AS, Swalla BJ. Head regeneration in
681 hemichordates is not a strict recapitulation of development: Head Regeneration in

682 Hemichordates. Dev Dyn. 2016 Dec;245(12):1159–75.

683 34. Vizcaya-Molina E, Klein CC, Serras F, Mishra RK, Guigó R, Corominas M.
684 Damage-responsive elements in *Drosophila* regeneration. Genome Res. 2018
685 Dec;28(12):1852–66.

686 35. Sun G, Irvine KD. Control of Growth During Regeneration. In: Current Topics in
687 Developmental Biology [Internet]. Elsevier; 2014 [cited 2019 Feb 27]. p. 95–120.
688 Available from: https://linkinghub.elsevier.com/retrieve/pii/B9780123914989000036

689 36. Hariharan IK, Serras F. Imaginal disc regeneration takes flight. Curr Opin Cell
690 Biol. 2017 Oct;48:10–6.

691 37. Sonoda J. Drosophila Brain Tumor is a translational repressor. Genes Dev. 2001
692 Mar 15;15(6):762–73.

693 38. Loedige I, Stotz M, Qamar S, Kramer K, Hennig J, Schubert T, et al. The NHL
694 domain of BRAT is an RNA-binding domain that directly contacts the hunchback mRNA
695 for regulation. Genes Dev. 2014 Apr 1;28(7):749–64.

696 39. Loedige I, Jakob L, Treiber T, Ray D, Stotz M, Treiber N, et al. The Crystal
697 Structure of the NHL Domain in Complex with RNA Reveals the Molecular Basis of
698 Drosophila Brain-Tumor-Mediated Gene Regulation. Cell Rep. 2015 Nov;13(6):1206–
699 20.

700 40. Arama E, Dickman D, Kimchie Z, Shearn A, Lev Z. Mutations in the β-propeller
701 domain of the Drosophila brain tumor (brat) protein induce neoplasm in the larval brain.
702 Oncogene. 2000;19(33):3706.

703 41. Harris RE, Pargett M, Sutcliffe C, Umulis D, Ashe HL. Brat Promotes Stem Cell
704 Differentiation via Control of a Bistable Switch that Restricts BMP Signaling. Dev Cell.
705 2011 Jan;20(1):72–83.

706 42. Betschinger J, Mechtler K, Knoblich JA. Asymmetric Segregation of the Tumor
707 Suppressor Brat Regulates Self-Renewal in Drosophila Neural Stem Cells. Cell. 2006
708 Mar;124(6):1241–53.

709 43. Lee C-Y, Wilkinson BD, Siegrist SE, Wharton RP, Doe CQ. Brat Is a Miranda
710 Cargo Protein that Promotes Neuronal Differentiation and Inhibits Neuroblast Self-
711 Renewal. Dev Cell. 2006 Apr;10(4):441–9.

712 44. Chen G, Kong J, Tucker-Burden C, Anand M, Rong Y, Rahman F, et al. Human
713 Brat Ortholog TRIM3 Is a Tumor Suppressor That Regulates Asymmetric Cell Division
714 in Glioblastoma. Cancer Res. 2014 Aug 15;74(16):4536–48.

715 45. Schwamborn JC, Berezikov E, Knoblich JA. The TRIM-NHL Protein TRIM32
716 Activates MicroRNAs and Prevents Self-Renewal in Mouse Neural Progenitors. Cell.
717 2009 Mar;136(5):913–25.

718 46. Nicklas S, Otto A, Wu X, Miller P, Stelzer S, Wen Y, et al. TRIM32 Regulates
719 Skeletal Muscle Stem Cell Differentiation and Is Necessary for Normal Adult Muscle
720 Regeneration. PLOS ONE. 2012 Jan 27;7(1):e30445.

721 47. Kudryashova E, Kramerova I, Spencer MJ. Satellite cell senescence underlies
722 myopathy in a mouse model of limb-girdle muscular dystrophy 2H. J Clin Invest. 2012
723 May 1;122(5):1764–76.

724 48. Vonesch SC, Lamparter D, Mackay TFC, Bergmann S, Hafen E. Genome-Wide
725 Analysis Reveals Novel Regulators of Growth in Drosophila melanogaster. Barsh GS,
726 editor. PLOS Genet. 2016 Jan 11;12(1):e1005616.

727 49. Skinner A, Khan SJ, Smith-Bolton RK. Trithorax regulates systemic signaling
728 during *Drosophila* imaginal disc regeneration. Development. 2015 Oct
729 15;142(20):3500–11.

730 50. Khan SJ, Abidi SNF, Skinner A, Tian Y, Smith-Bolton RK. The Drosophila Duox
731 maturation factor is a key component of a positive feedback loop that sustains
732 regeneration signaling. Bosco G, editor. PLOS Genet. 2017 Jul 28;13(7):e1006937.

733 51. Brock AR, Seto M, Smith-Bolton RK. Cap-n-Collar Promotes Tissue
734 Regeneration by Regulating ROS and JNK Signaling in the *Drosophila melanogaster*
735 Wing Imaginal Disc. Genetics. 2017 Jul;206(3):1505–20.

736 52. Luschnig S, Moussian B, Krauss J, Desjeux I, Perkovic J, Nüsslein-Volhard C.
737 An F1 genetic screen for maternal-effect mutations affecting embryonic pattern
738 formation in Drosophila melanogaster. Genetics. 2004;167(1):325–42.

739 53. Wright TR, Beermann W, Marsh JL, Bishop CP, Steward R, Black BC, et al. The
740 genetics of dopa decarboxylase in Drosophila melanogaster. Chromosoma.
741 1981;83(1):45–58.

742 54. Parks AL, Cook KR, Belvin M, Dompe NA, Fawcett R, Huppert K, et al.
743 Systematic generation of high-resolution deletion coverage of the Drosophila
744 melanogaster genome. Nat Genet. 2004 Mar;36(3):288–92.

745 55. Stathakis DG. The Genetic and Molecular Organization of the Dopa
746 Decarboxylase Gene Cluster of Drosophila Melanogaster. Genetics. 1995;141(2):629–
747 55.

748 56. Ferreira A, Boulan L, Perez L, Milán M. Mei-P26 Mediates Tissue-Specific
749 Responses to the Brat Tumor Suppressor and the dMyc Proto-Oncogene in *Drosophila*.
750 Genetics. 2014 Sep;198(1):249–58.

751 57. Halme A, Cheng M, Hariharan IK. Retinoids Regulate a Developmental
752 Checkpoint for Tissue Regeneration in Drosophila. Curr Biol. 2010 Mar;20(5):458–63.

753 58. Colombani J. Secreted Peptide Dilp8 Coordinates Drosophila Tissue Growth with
754 Developmental Timing. Science. 2012;336(6081):582–5.

755 59. Garelli A, Gontijo AM, Miguela V, Caparros E, Dominguez M. Imaginal discs
756 secrete insulin-like peptide 8 to mediate plasticity of growth and maturation. Science.
757 2012;336(6081):579–82.

758 60. Abbott LC, Karpen GH, Schubiger G. Compartmental restrictions and blastema
759 formation during pattern regulation in Drosophila imaginal leg discs. Dev Biol.
760 1981;87(1):64–75.

761 61. Ng M, Diaz-Benjumea FJ, Cohen SM. Nubbin encodes a POU-domain protein
762 required for proximal-distal patterning in the Drosophila wing. Development.
763 1995;121(2):589–99.

764 62. Komori H, Xiao Q, McCartney BM, Lee C-Y. Brain tumor specifies intermediate
765 progenitor cell identity by attenuating -catenin/Armadillo activity. Development. 2014

766 Jan 1;141(1):51–62.

767 63. Couso JP, Bate M, Martinez-Arias A. A wingless-dependent polar coordinate
768 system in Drosophila imaginal discs. Science. 1993;259(5094):484–9.

769 64. Wu DC, Johnston LA. Control of Wing Size and Proportions by Drosophila Myc.
770 Genetics. 2010 Jan;184(1):199–211.

771 65. Diaz-Benjumea FJ, Cohen SM. Interaction between dorsal and ventral cells in
772 the imaginal disc directs wing development in Drosophila. Cell. 1993;75(4):741–52.

773 66. Micchelli CA, Rulifson EJ, Blair SS. The function and regulation of cut expression
774 on the wing margin of Drosophila: Notch, Wingless and a dominant negative role for
775 Delta and Serrate. Development. 1997;124(8):1485–95.

776 67. Becam I, Milán M. A permissive role of Notch in maintaining the DV affinity
777 boundary of the Drosophila wing. Dev Biol. 2008 Oct;322(1):190–8.

778 68. Saj A, Arziman Z, Stempfle D, van Belle W, Sauder U, Horn T, et al. A Combined
779 Ex Vivo and In Vivo RNAi Screen for Notch Regulators in Drosophila Reveals an
780 Extensive Notch Interaction Network. Dev Cell. 2010 May;18(5):862–76.

781 69. Mukherjee S, Tucker-Burden C, Zhang C, Moberg K, Read R, Hadjipanayis C, et
782 al. *Drosophila* Brat and Human Ortholog TRIM3 Maintain Stem Cell Equilibrium and
783 Suppress Brain Tumorigenesis by Attenuating Notch Nuclear Transport. Cancer Res.
784 2016 Apr 15;76(8):2443–52.

785 70. Bray SJ. Notch signalling: a simple pathway becomes complex. Nat Rev Mol Cell
786 Biol. 2006 Sep;7(9):678–89.

787 71. Couso JP, Bishop SA, Arias AM. The wingless signalling pathway and the
788 patterning of the wing margin in Drosophila. Development. 1994;120(3):621–36.

789 72. Jack J, Dorsett D, Delotto Y, Liu S. Expression of the cut locus in the Drosophila
790 wing margin is required for cell type specification and is regulated by a distant
791 enhancer. Development. 1991;113(3):735–47.

792 73. Pierce SB. dMyc is required for larval growth and endoreplication in Drosophila.
793 Development. 2004 Apr 21;131(10):2317–27.

794 74. Bosch JA, Sumabat TM, Hariharan IK. Persistence of RNAi-Mediated
795 Knockdown in *Drosophila* Complicates Mosaic Analysis Yet Enables Highly Sensitive
796 Lineage Tracing. Genetics. 2016 May;203(1):109–18.

797 75. Dillard C, Narbonne-Reveau K, Foppolo S, Lanet E, Maurange C. Two distinct
798 mechanisms silence *chinmo* in *Drosophila* neuroblasts and neuroepithelial cells to limit
799 their self-renewal. Development. 2018 Jan 15;145(2):dev154534.

800 76. Flaherty MS, Salis P, Evans CJ, Ekas LA, Marouf A, Zavadil J, et al. chinmo Is a
801 Functional Effector of the JAK/STAT Pathway that Regulates Eye Development, Tumor
802 Formation, and Stem Cell Self-Renewal in Drosophila. Dev Cell. 2010 Apr;18(4):556–
803 68.

804 77. Narbonne-Reveau K, Maurange C. Developmental regulation of regenerative
805 potential in Drosophila by ecdysone through a bistable loop of ZBTB transcription
806 factors. PLOS Biol. 2019;17(2):e3000149.

807 78. Kudron MM, Victorsen A, Gevirtzman L, Hillier LW, Fisher WW, Vafeados D, et

al. The ModERN Resource: Genome-Wide Binding Profiles for Hundreds of Drosophila and Caenorhabditis elegans Transcription Factors. Genetics. 2018;208(3):937–49.

79. Amati B, Land H. Myc—Max—Mad: a transcription factor network controlling cell cycle progression, differentiation and death. Curr Opin Genet Dev. 1994;4(1):102–8.

80. Takahashi K, Yamanaka S. Induction of Pluripotent Stem Cells from Mouse Embryonic and Adult Fibroblast Cultures by Defined Factors. Cell. 2006 Aug;126(4):663–76.

81. Hayashi R, Goto Y, Ikeda R, Yokoyama KK, Yoshida K. CDCA4 Is an E2F Transcription Factor Family-induced Nuclear Factor That Regulates E2F-dependent Transcriptional Activation and Cell Proliferation. J Biol Chem. 2006 Nov 24;281(47):35633–48.

82. Hsu SI-H, Yang CM, Sim KG, Hentschel DM, O'Leary E, Bonventre JV. TRIP-Br: a novel family of PHD zinc finger- and bromodomain-interacting proteins that regulate the transcriptional activity of E2F-1/DP-1. EMBO J. 2001 May 1;20(9):2273–85.

83. Watanabe-Fukunaga R, Iida S, Shimizu Y, Nagata S, Fukunaga R. SEI family of nuclear factors regulates p53-dependent transcriptional activation. Genes Cells. 2005;10(8):851–60.

84. Calgaro S, Boube M, Cribbs DL, Bourbon H-M. The Drosophila gene taranis encodes a novel trithorax group member potentially linked to the cell cycle regulatory apparatus. Genetics. 2002;160(2):547–60.

85. Laver JD, Li X, Ray D, Cook KB, Hahn NA, Nabeel-Shah S, et al. Brain tumor is

829 a sequence-specific RNA-binding protein that directs maternal mRNA clearance during
830 the Drosophila maternal-to-zygotic transition. Genome Biol [Internet]. 2015 Dec [cited
831 2019 Feb 28];16(1). Available from: http://genomebiology.com/2015/16/1/94

832 86. Komori H, Golden KL, Kobayashi T, Kageyama R, Lee C-Y. Multilayered gene
833 control drives timely exit from the stem cell state in uncommitted progenitors during
834 Drosophila asymmetric neural stem cell division. Genes Dev. 2018 Dec 1;32(23-
835 24):1550–61.

836 87. Hazelrigg T, Levis R, Rubin GM. Transformation of white locus DNA in
837 drosophila: dosage compensation, zeste interaction, and position effects. Cell.
838 1984;36(2):469–81.

839 88. Wright TR, Bewley GC, Sherald AF. The genetics of dopa decarboxylase in
840 Drosophila melanogaster. II. Isolation and characterization of dopa-decarboxylase-
841 deficient mutants and their relationship to the α-methyl-dopa-hypersensitive mutants.
842 Genetics. 1976;84(2):287–310.

843 89. Cohen B, McGuffin ME, Pfeifle C, Segal D, Cohen SM. apterous, a gene required
844 for imaginal disc development in Drosophila encodes a member of the LIM family of
845 developmental regulatory proteins. Genes Dev. 1992;6(5):715–29.

846 90. Littleton JT, Bellen HJ. Genetic and Phenotypic Analysis of Thirteen Essential
847 Genes in Cytological Interval 22f1-2; 23b1-2 Reveals Novel Genes Required for Neural
848 Development in Drosophila. Genetics. 1994 Sep;138(1):111–23.

849 91. Johnston LA, Prober DA, Edgar BA, Eisenman RN, Gallant P. Drosophila myc

regulates cellular growth during development. Cell. 1999;98(6):779–90.

92. Oh H, Irvine KD. In vivo regulation of Yorkie phosphorylation and localization. Development. 2008 Feb 6;135(6):1081–8.

93. Dietzl G, Chen D, Schnorrer F, Su K-C, Barinova Y, Fellner M, et al. A genome-wide transgenic RNAi library for conditional gene inactivation in Drosophila. Nature. 2007 Jul;448(7150):151–6.

94. Averof M. Evolutionary origin of insect wings from ancestral gills. Nature. 6617(385):627–30.

95. Classen A-K, Bunker BD, Harvey KF, Vaccari T, Bilder D. A tumor suppressor activity of Drosophila Polycomb genes mediated by JAK-STAT signaling. Nat Genet. 2009 Oct;41(10):1150–5.

Fig 1

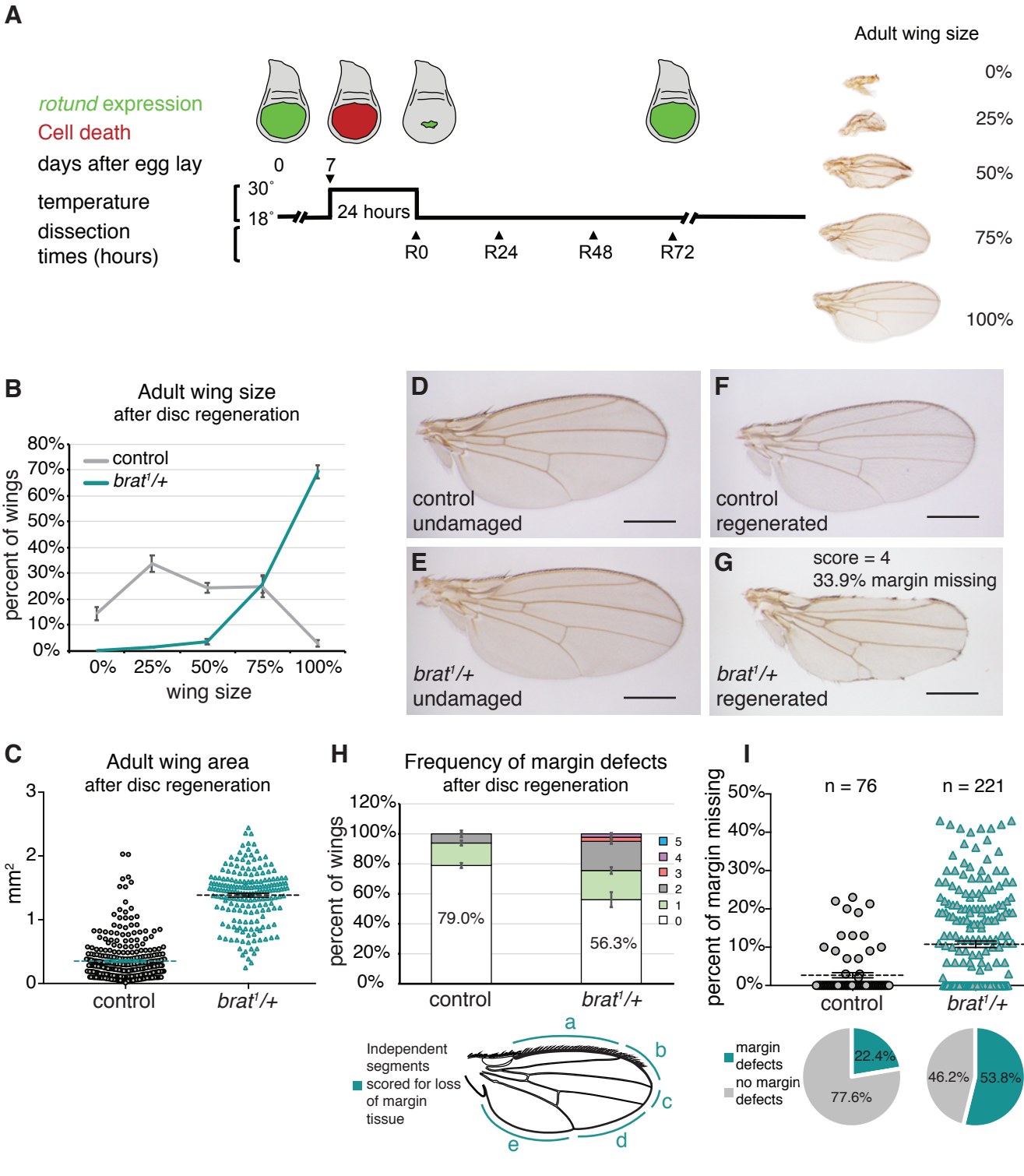
A
Adult wing size
0%
25%
50%
75%
100%
rotund expression
Cell death
days after egg lay
0
7
temperature
30˚
18˚
24 hours
dissection times (hours)
R0
R24
R48
R72
B
Adult wing size
after disc regeneration
percent of wings
control
brat1/+
wing size
D
control
undamaged
F
control
regenerated
E
brat1/+
undamaged
G
score = 4
33.9% margin missing
brat1/+
regenerated
C
Adult wing area
after disc regeneration
mm2
control
brat1/+
H
Frequency of margin defects
after disc regeneration
percent of wings
79.0%
56.3%
Independent segments scored for loss of margin tissue
a
b
c
d
e
I
n = 76
n = 221
percent of margin missing
margin defects
no margin defects
22.4%
77.6%
46.2%
53.8%

Fig 1. Enhanced regenerative growth and wing margin cell-fate specification defects in *brat*^{1}/+ during regeneration.

(A) The protocol used to study regeneration. Animals were raised at 18°C and shifted to 30°C for 24 hours during early third-instar larval development on day 7 after egg lay (AEL). Larvae were returned to 18°C and were dissected at the time points noted during recovery (R) or allowed to pupariate and eclose. Representative wings depicting the range of adult wing sizes observed after regeneration compared to the size of a normal wing are shown. (B) Adult wing sizes observed after disc regeneration for control (w^{1118}) (n = 317) and *brat*^{1}/+ (n = 208) wings, from three independent experiments. (C) Adult wing area after disc regeneration, measured using ImageJ after mounting and imaging wings, for control (w^{1118}) (n = 309) and *brat*^{1}/+ (n = 195) wings. p = 2.5158E-119. Wings in (C) are from the same experiments as (B). Note that number of wings in (C) is less for both control and *brat*^{1}/+ due to some wings being damaged during the mounting process. (D) Undamaged control (w^{1118}) wing. (E) Undamaged *brat*^{1}/+ wing. (F) Adult control (w^{1118}) wing after disc regeneration. (G) Adult *brat*^{1}/+ wing after disc regeneration. (H) Frequency of margin defects seen in adult wings after disc regeneration for control (w^{1118}) (n = 93) and *brat*^{1}/+ (n = 218) wings, from three independent experiments. The wing margin was divided into five segments based on where the veins intersect the margin as shown in the diagram. Each wing was scored for the number of segments that had some margin tissue missing, with wings with a perfectly intact margin scoring at zero. Wing shown in (G) had tissue missing in four segments. (I) Margin tissue lost as a percentage of total wing perimeter for control (w^{1118}) (n = 76) and *brat*^{1}/+ (n = 221) wings. p = 9.947E-08. The margin perimeter and

the length of margin tissue lost were measured using ImageJ after mounting and imaging wings. Wings in (I) are from the same experiments as (H). Note that number of wings in the two quantifications is different because we did not quantify wings with length <1.1 mm for males and <1.7 mm for females, to ensure analysis was being carried out on nearly fully regenerated wings. (I). Percentage of wings with no defects fell from 79.0% to 77.6% for control and from 56.3% to 53.8% for *brat*^{1}/+ wings due to the increased ability to detect lost margin tissue at the higher magnification and resolution achieved by imaging the wings. Wing shown in (G) had 33.9% of margin tissue missing. Error bars mark standard error of the mean (SEM). Student's T-test used for statistical analyses. Scale bars are 0.5 mm.

Fig 2

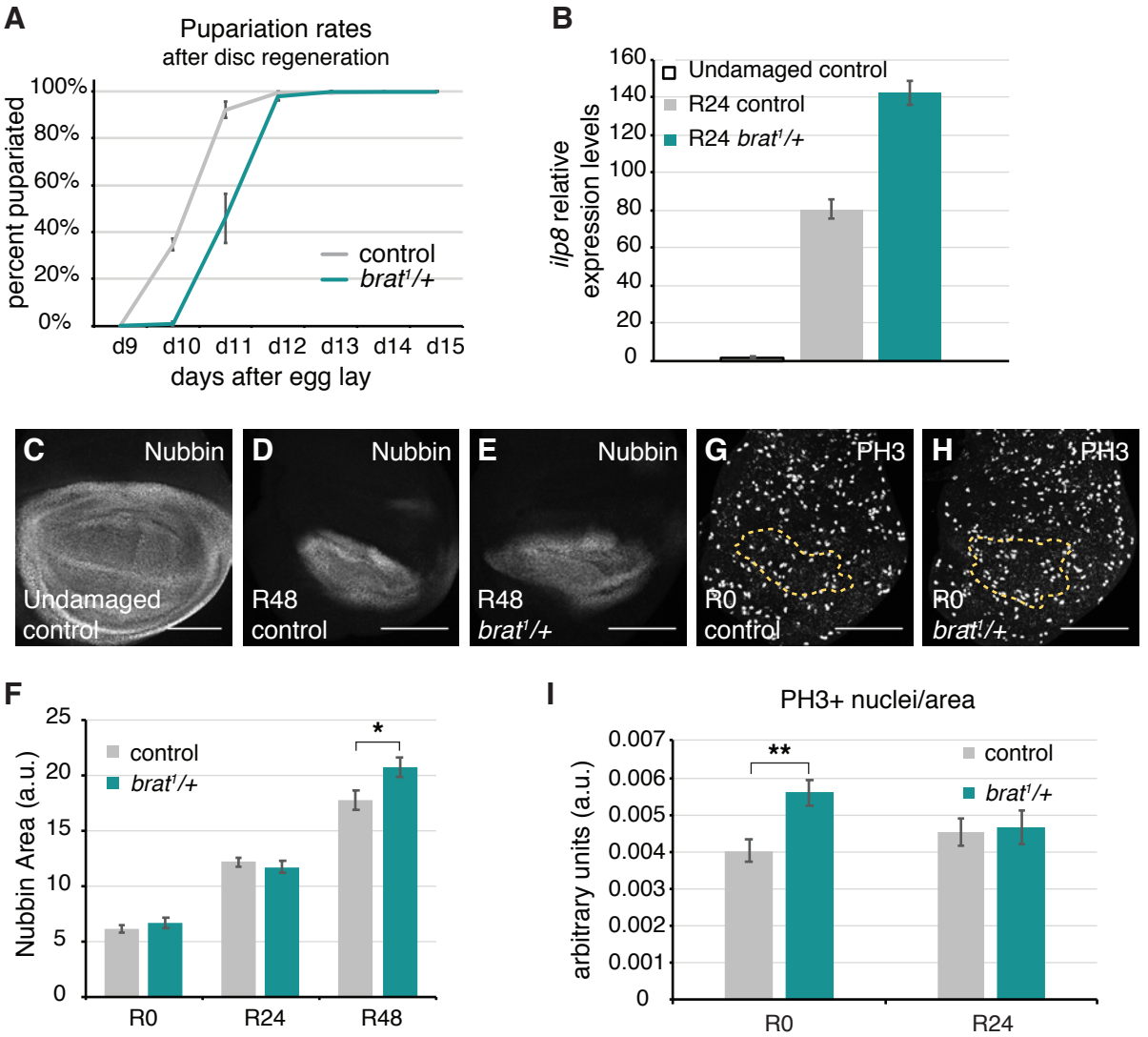
A
Pupariation rates
after disc regeneration
percent pupariated
100%
80%
60%
40%
20%
0%
d9
d10
d11
d12
d13
d14
d15
days after egg lay
control
brat1/+
B
ilp8 relative expression levels
160
140
120
100
80
60
40
20
0
Undamaged control
R24 control
R24 brat1/+
C
Nubbin
Undamaged control
D
Nubbin
R48 control
E
Nubbin
R48 brat1/+
G
PH3
R0 control
H
PH3
R0 brat1/+
F
Nubbin Area (a.u.)
25
20
15
10
5
0
control
brat1/+
*
R0
R24
R48
I
PH3+ nuclei/area
arbitrary units (a.u.)
0.007
0.006
0.005
0.004
0.003
0.002
0.001
0
**
control
brat1/+
R0
R24

Fig 2. *brat*^{1}/+ animals have a regenerative growth advantage.

(A) Pupariation rates after disc regeneration for control (w^{1118}) (n = 384) and *brat*^{1}/+ (n = 107) animals, from three independent experiments. (B) Relative expression levels of *ilp8* for undamaged control (*rnGAL4, tubGAL80ts/TM6B* females crossed to w^{1118} males and shifted to 30˚C for 24 hours at 7 days AEL), R24 control (w^{1118}) and R24 *brat*^{1}/+ discs. (C) Anti-Nubbin immunostaining in an undamaged control disc. (D-E) Anti-Nubbin immunostaining in an R48 control (w^{1118}) disc (D), and an R48 *brat*^{1}/+ disc (E). (F) Quantification of area of Nubbin-expressing cells for control (w^{1118}) and *brat*^{1}/+ discs at R0 (n = 10 and 10), R24 (n = 12 and 12) and R48 (n = 10 and 10). * $p < 0.03$. (G-H) Anti-PH3 immunostaining in an R0 control (w^{1118}) disc (G), and an R0 *brat*^{1}/+ disc (H). The yellow dashed lines outline the Nubbin-expressing wing pouch. (I) PH3-positive nuclei were counted within the regenerating tissue as marked by Anti-Nubbin co-immunostaining. Quantification of PH3-positive nuclei in Nubbin area for control (w^{1118}) and *brat*^{1}/+ discs at R0 (n = 16 and 18) and R24 (n = 15 and 16). ** $p < 0.002$. Error bars represent SEM. Student's T-test used for statistical analyses. Scale bars are 100 μm.

Fig 3

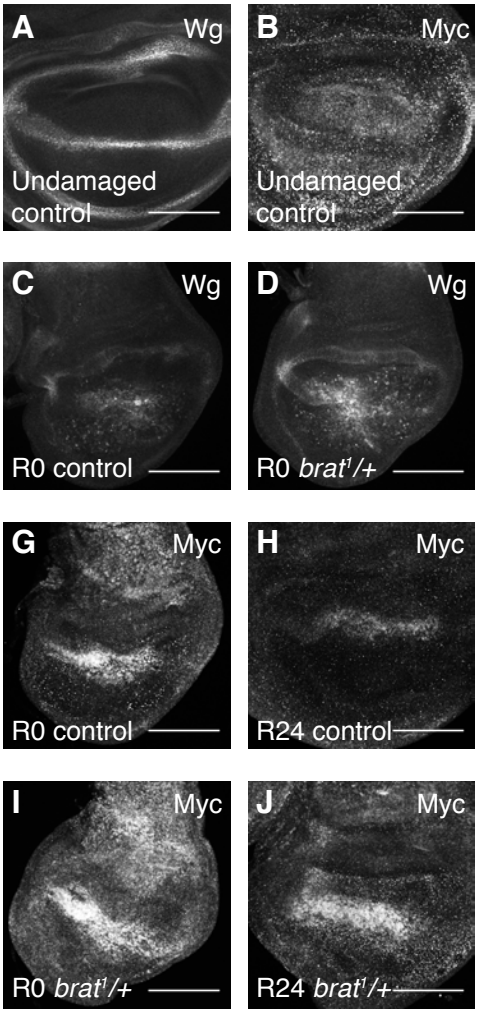
A
Wg
Undamaged control
B
Myc
Undamaged control
C
Wg
R0 control
D
Wg
R0 brat1/+
G
Myc
R0 control
H
Myc
R24 control
I
Myc
R0 brat1/+
J
Myc
R24 brat1/+

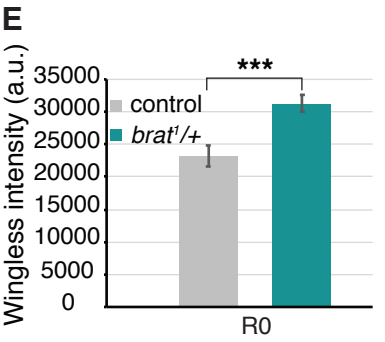
E
Wingless intensity (a.u.)
35000
30000
25000
20000
15000
10000
5000
0
control
brat1/+
***
R0

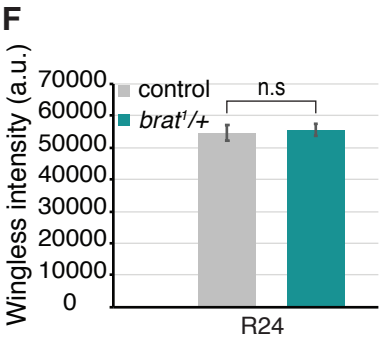
F
Wingless intensity (a.u.)
70000
60000
50000
40000
30000
20000
10000
0
control
brat1/+
n.s
R24

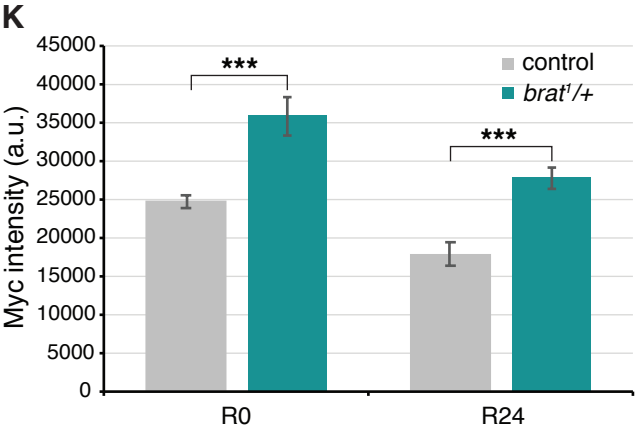
K
Myc intensity (a.u.)
45000
40000
35000
30000
25000
20000
15000
10000
5000
0
control
brat1/+
***
***
R0
R24

Fig 3. *brat*^{1}/+ animals experience elevated regeneration signaling.

(A) Anti-Wg immunostaining in an undamaged control (*w*^{1118}) disc. (B) Anti-Myc immunostaining in an undamaged control (*w*^{1118}) disc. (C-D) Anti-Wg immunostaining in an R0 control (*w*^{1118}) disc (C) and an R0 *brat*^{1}/+ disc (D). (E) Quantification of Wg fluorescence intensity in R0 control (*w*^{1118}) (n = 13) and R0 *brat*^{1}/+ (n = 17) discs. *** $p < 0.0006$. (F) Quantification of Wg fluorescence intensity in R24 control (*w*^{1118}) (n = 12) and R24 *brat*^{1}/+ (n = 11) discs. Area for fluorescence intensity measurement was defined by the Wg expression domain in the wing pouch. (G-J) Anti-Myc immunostaining in an R0 control (*w*^{1118}) disc (G), an R24 control (*w*^{1118}) disc (H), an R0 *brat*^{1}/+ disc (I) and an R24 *brat*^{1}/+ disc (J). (K) Quantification of Myc fluorescence intensity in R0 control (*w*^{1118}) (n = 13), R0 *brat*^{1}/+ (n = 12), R24 control (*w*^{1118}) (n = 13), and R24 *brat*^{1}/+ (n = 12) discs. Area for fluorescence intensity measurement was defined by the elevated Myc expression domain in the wing pouch. R0 *** $p < 0.0003$, R24 *** $p < 0.0001$. Error bars represent SEM. Student's T-test used for statistical analyses. Scale bars are 100 μm.

Fig 4

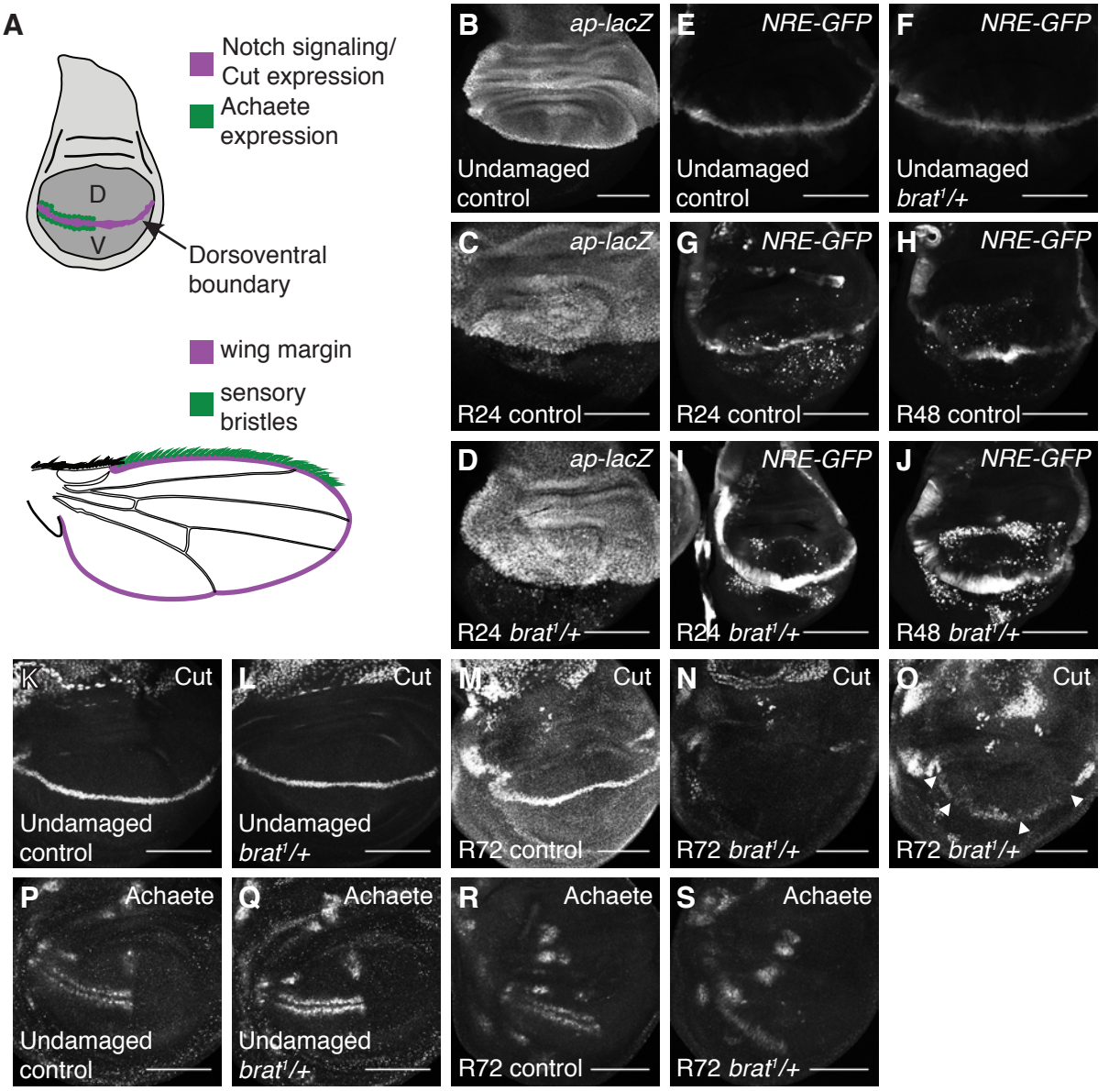
A
Notch signaling/
Cut expression
Achaete
expression
D
V
Dorsoventral
boundary
wing margin
sensory
bristles
B ap-lacZ
Undamaged
control
E NRE-GFP
Undamaged
control
F NRE-GFP
Undamaged
brat1/+
C ap-lacZ
R24 control
G NRE-GFP
R24 control
H NRE-GFP
R48 control
D ap-lacZ
R24 brat1/+
I NRE-GFP
R24 brat1/+
J NRE-GFP
R48 brat1/+
K Cut
Undamaged
control
L Cut
Undamaged
brat1/+
M Cut
R72 control
N Cut
R72 brat1/+
O Cut
R72 brat1/+
P Achaete
Undamaged
control
Q Achaete
Undamaged
brat1/+
R Achaete
R72 control
S Achaete
R72 brat1/+

Fig 4. *Brat* regulates margin cell-fate specification.

(A) Drawings of a wing imaginal disc and an adult wing. D = dorsal and V = ventral compartments of the wing disc, with the dorsoventral boundary marked in purple. Notch signaling and Cut expression are present at the dorsoventral boundary, which forms the adult wing margin, also marked in purple. Achaete-expressing cells, marked in green, give rise to the sensory bristles at the anterior half of the margin in the adult wing, also marked in green. (B) *ap-lacZ* expression in an undamaged control disc from a third-instar *ap-lacZ/CyO* animal. (C-D) *ap-lacZ* expression in an R24 control (w^{1118}) disc (C) and an R24 $brat^{1}$/+ disc (D). (E-F) *NRE-GFP* expression in an undamaged control (w^{1118}) disc (E) and an undamaged $brat^{1}$/+ disc (F). (G-J) *NRE-GFP* expression in an R0 control (w^{1118}) disc (G), an R24 control (w^{1118}) disc (H), an R0 $brat^{1}$/+ disc (I) and an R24 $brat^{1}$/+ disc (J). (K-L) Anti-Ct immunostaining in an undamaged control (w^{1118}) disc (K) and an undamaged $brat^{1}$/+ disc (L). (M-O) Anti-Ct immunostaining in an R72 control (w^{1118}) disc (M) and an R72 $brat^{1}$/+ discs (N-O). Arrowheads point to loss of Ct expression in (O). (P-Q) Anti-Ac immunostaining in an undamaged control (w^{1118}) disc (P) and an undamaged $brat^{1}$/+ disc (Q). (R-S) Anti-Ac immunostaining in an R72 control (w^{1118}) disc (R) and an R72 $brat^{1}$/+ disc (S). Scale bars are 100 μm.

Fig 5

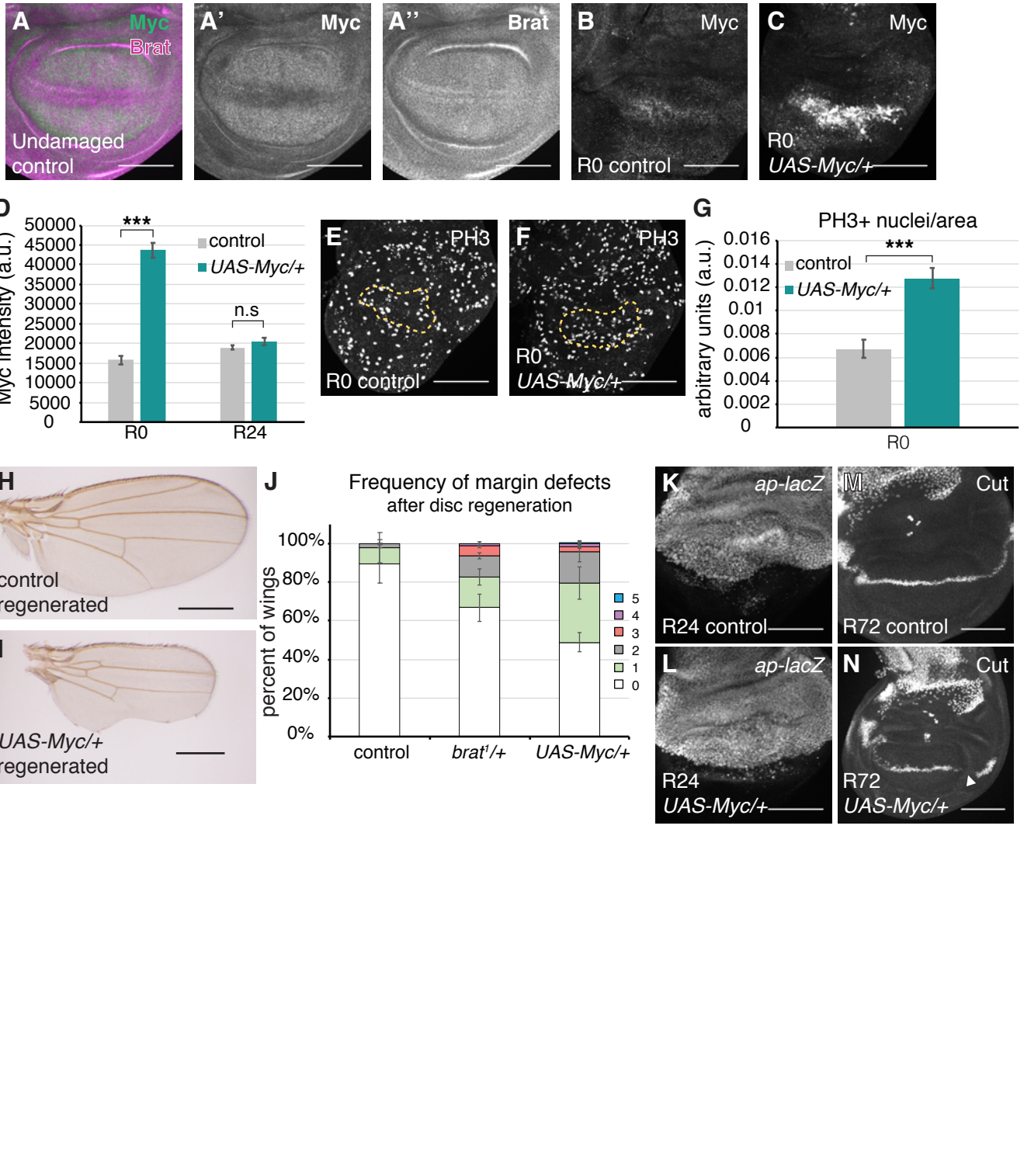
A
Myc
Brat
Undamaged
control
A'
Myc
A''
Brat
B
Myc
R0 control
C
Myc
R0
UAS-Myc/+
D
Myc intensity (a.u.)
50000
45000
40000
35000
30000
25000
20000
15000
10000
5000
0
***
n.s
control
UAS-Myc/+
R0
R24
E
PH3
R0 control
F
PH3
R0
UAS-Myc/+
G
PH3+ nuclei/area
arbitrary units (a.u.)
0.016
0.014
0.012
0.01
0.008
0.006
0.004
0.002
0
***
control
UAS-Myc/+
R0
H
control
regenerated
I
UAS-Myc/+
regenerated
J
Frequency of margin defects
after disc regeneration
percent of wings
100%
80%
60%
40%
20%
0%
5
4
3
2
1
0
control
brat1/+
UAS-Myc/+
K
ap-lacZ
R24 control
M
Cut
R72 control
L
ap-lacZ
R24
UAS-Myc/+
N
Cut
R72
UAS-Myc/+

Fig 5. High Myc expression causes margin defects.

(A-A'') Anti-Myc and Anti-Brat co-immunostaining in an undamaged control disc. *rnGAL4, GAL80^{ts}/attP2* animals were shifted to 30°C on day 7 AEL and dissected 24 hours later. (B-C) Anti-Myc immunostaining in an R0 control (*w^{1118}*) disc (B) and an R0 *UAS-Myc/+* disc (C). (D) Quantification of Myc fluorescence intensity in R0 control (*w^{1118}*) (n = 13), R0 *UAS-Myc/+* (n = 12), R24 control (*w^{1118}*) (n = 13), and R24 *UAS-Myc/+* (n = 12) discs. Area for fluorescence intensity measurement was defined by the elevated Myc expression domain in the wing pouch. *** p = 1.2E-11. (E-F) Anti-PH3 immunostaining in an R0 control (*w^{1118}*) disc (E), and an R0 *UAS-Myc/+* disc (F). The yellow dashed lines outline the Nubbin-expressing wing pouch. (G) PH3-positive nuclei were counted within the regenerating wing pouch as marked by Anti-Nubbin co-immunostaining. Quantification of PH3-positive nuclei in the Nubbin area for R0 control (*w^{1118}*) (n = 15) and *UAS-Myc/+* (n = 15) discs. *** p < 0.00002. (H) Adult control (*w^{1118}*) wing after disc regeneration. (I) Adult *UAS-Myc/+* wing after disc regeneration. (J) Frequency of margin defects, as quantified in Fig 1H, seen in adult wings after disc regeneration for control (*w^{1118}*) (n = 134), *brat^{1}/+* (n = 193) and *UAS-Myc/+* (n = 200) wings, from three independent experiments. (K-L) *ap-lacZ* expression in an R24 control (*w^{1118}*) disc (K) and an R24 *UAS-Myc/+* disc (L). (M-N) Anti-Ct immunostaining in an R72 control (*w^{1118}*) disc (M) and an R72 *UAS-Myc/+* disc (N). Error bars represent SEM. Student's T-test used for statistical analyses. Scale bars are 100 μm.

Fig 6

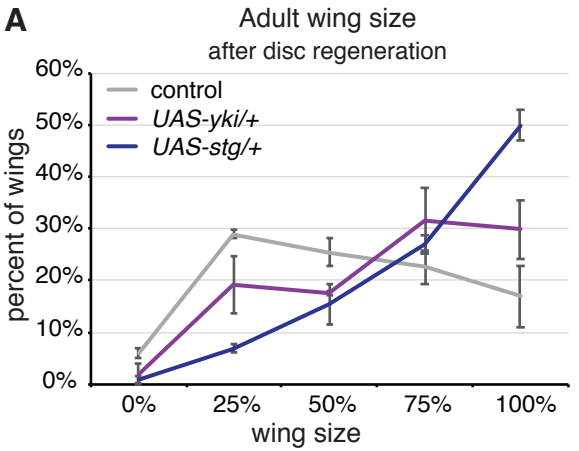
A
Adult wing size
after disc regeneration
60%
50%
40%
30%
20%
10%
0%
percent of wings
control
UAS-yki/+
UAS-stg/+
0%
25%
50%
75%
100%
wing size

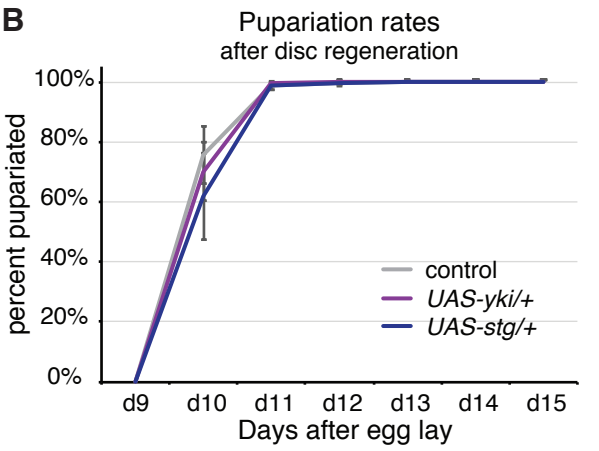
B
Pupariation rates
after disc regeneration
100%
80%
60%
40%
20%
0%
percent pupariated
control
UAS-yki/+
UAS-stg/+
d9
d10
d11
d12
d13
d14
d15
Days after egg lay

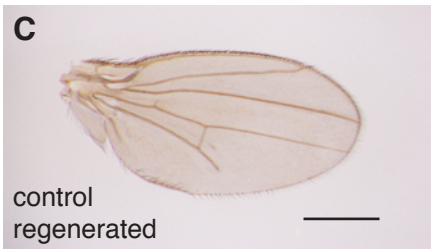
C
control
regenerated

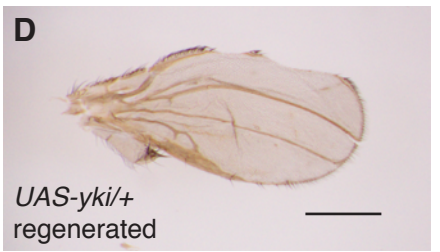
D
UAS-yki/+
regenerated

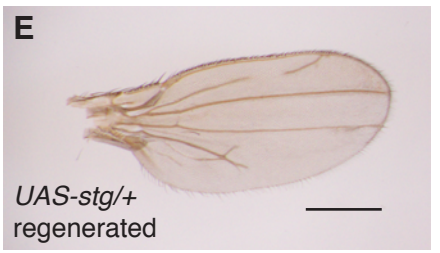
E
UAS-stg/+
regenerated

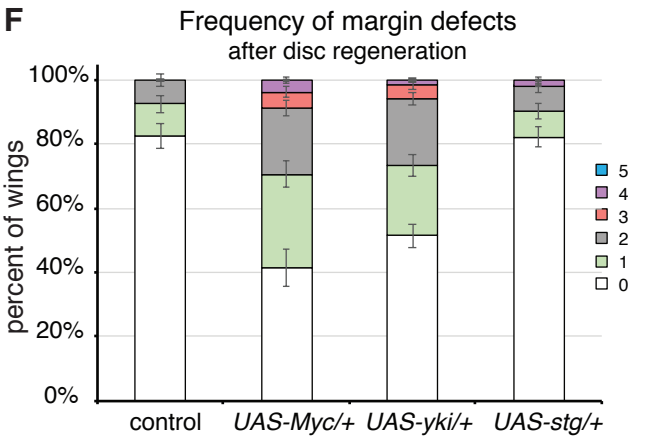
F
Frequency of margin defects
after disc regeneration
100%
80%
60%
40%
20%
0%
percent of wings
5
4
3
2
1
0
control
UAS-Myc/+
UAS-yki/+
UAS-stg/+

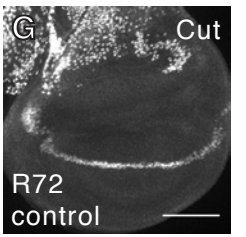
G
Cut
R72
control

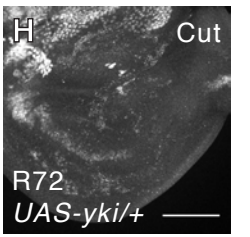
H
Cut
R72
UAS-yki/+

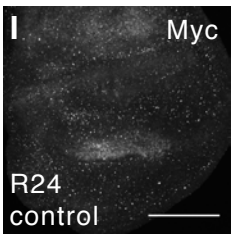
I
Myc
R24
control

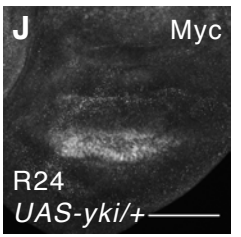
J
Myc
R24
UAS-yki/+

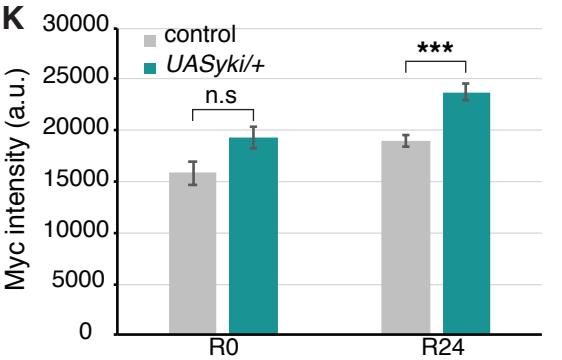
K
30000
25000
20000
15000
10000
5000
0
Myc intensity (a.u.)
control
UASyki/+
n.s
***
R0
R24

Fig 6. Overexpression of multiple growth-promoting genes can cause patterning defects.

(A) Adult wing sizes observed after disc regeneration for control (w^{1118}) (n = 420), *UAS-yki/+* (n = 463) and *UAS-stg/+* (n = 347) wings, from three independent experiments. (B) Pupariation rates after disc regeneration for control (w^{1118}) (n = 217), *UAS-yki/+* (n = 208) and *UAS-stg/+* (n = 210) wings, from three independent experiments. (C) Adult control (w^{1118}) wing after disc regeneration. (D) Adult *UAS-yki/+* wing after disc regeneration. (E) Adult *UAS-stg/+* wing after disc regeneration. (F) Frequency of margin defects seen in adult wings after disc regeneration for control (w^{1118}) (n = 209), *UAS-yki/+* (n = 357), and *UAS-stg/+* (n = 344) wings, from six independent experiments. (G-H) Anti-Ct immunostaining in an R72 control (w^{1118}) disc (G) and an R72 *UAS-yki/+* disc (H). (I-J) Anti-Myc immunostaining in an R24 control (w^{1118}) disc (I) and an R24 *UAS-yki/+* disc (J). (K) Quantification of Myc fluorescence intensity in R0 control (w^{1118}) (n = 13), R0 *UAS-yki/+* (n = 12), R24 control (w^{1118}) (n = 13), and R24 *UAS-yki/+* (n = 12) discs. Area for fluorescence intensity measurement was defined by the elevated Myc expression domain in the wing pouch. *** $p < 0.00004$. Error bars represent SEM. Student's T-test used for statistical analyses. Scale bars are 100 μm.

Fig 7

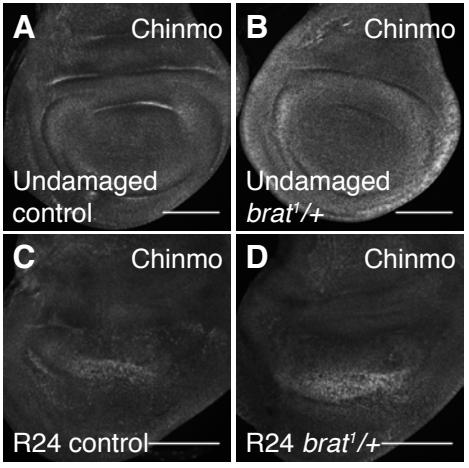
A
Chinmo
Undamaged
control
B
Chinmo
Undamaged
brat1/+
C
Chinmo
R24 control
D
Chinmo
R24 brat1/+

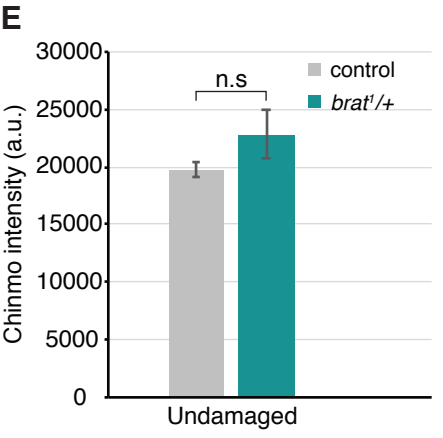
E
30000
25000
20000
15000
10000
5000
0
Chinmo intensity (a.u.)
n.s
control
brat1/+
Undamaged

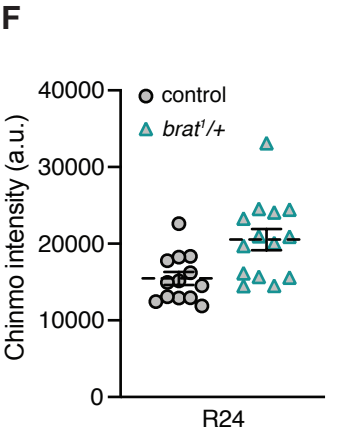
F
40000
30000
20000
10000
0
Chinmo intensity (a.u.)
control
brat1/+
R24

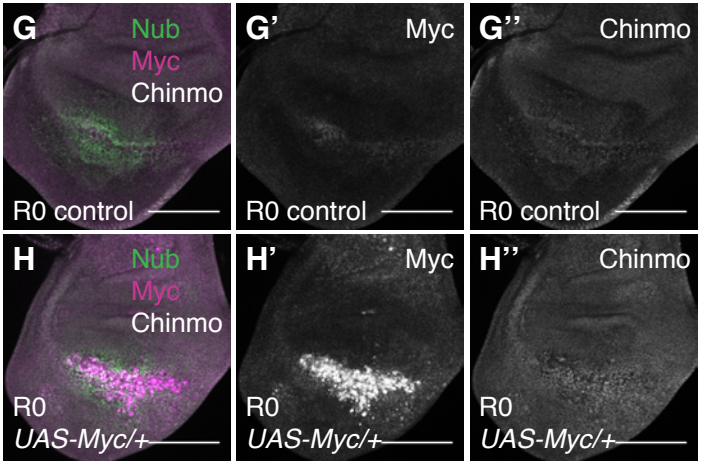
G
Nub
Myc
Chinmo
R0 control
G'
Myc
R0 control
G''
Chinmo
R0 control
H
Nub
Myc
Chinmo
R0
UAS-Myc/+
H'
Myc
R0
UAS-Myc/+
H''
Chinmo
R0
UAS-Myc/+

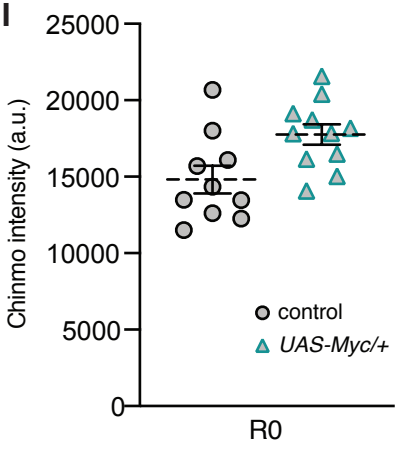
I
25000
20000
15000
10000
5000
0
Chinmo intensity (a.u.)
control
UAS-Myc/+
R0

Fig 7. Chinmo levels are elevated in *brat*^{1}/+ and Myc-overexpressing regenerating discs.

(A-B) Anti-Chinmo immunostaining in an undamaged control (*w*^{1118}) disc (A) and an undamaged *brat*^{1}/+ disc (B). (C-D) Anti-Chinmo immunostaining in an R24 control (*w*^{1118}) disc (C) and an R24 *brat*^{1}/+ disc (D). (E) Quantification of Chinmo fluorescence intensity in undamaged control (*w*^{1118}) (n = 11) and undamaged *brat*^{1}/+ (n = 10) discs. (F) Quantification of Chinmo fluorescence intensity in R24 control (*w*^{1118}) (n = 13) and R24 *brat*^{1}/+ (n = 14) discs. $p < 0.006$. Area for fluorescence intensity measurement was defined by the elevated Chinmo expression domain in the wing pouch. (G) Merge of anti-Nubbin, anti-Myc and anti-Chinmo immunostaining in an R0 control (*w*^{1118}) disc. (G'-G'') Same disc as (G) showing anti-Myc and anti-Chinmo immunostaining, respectively. (H) Merge of anti-Nubbin, anti-Myc and anti-Chinmo immunostaining in an R0 *brat*^{1}/+ disc. (H'-H'') Same disc as (H) showing anti-Myc and anti-Chinmo immunostaining, respectively. (I) Quantification of Chinmo fluorescence intensity in R0 control (*w*^{1118}) (n = 10) and R0 *UAS-Myc*/+ (n = 11) discs. $p < 0.02$. Area for fluorescence intensity measurement was defined by the elevated Myc expression domain in the wing pouch. Error bars represent SEM. Student's T-test used for statistical analyses. Scale bars are 100 μm.

Fig 8

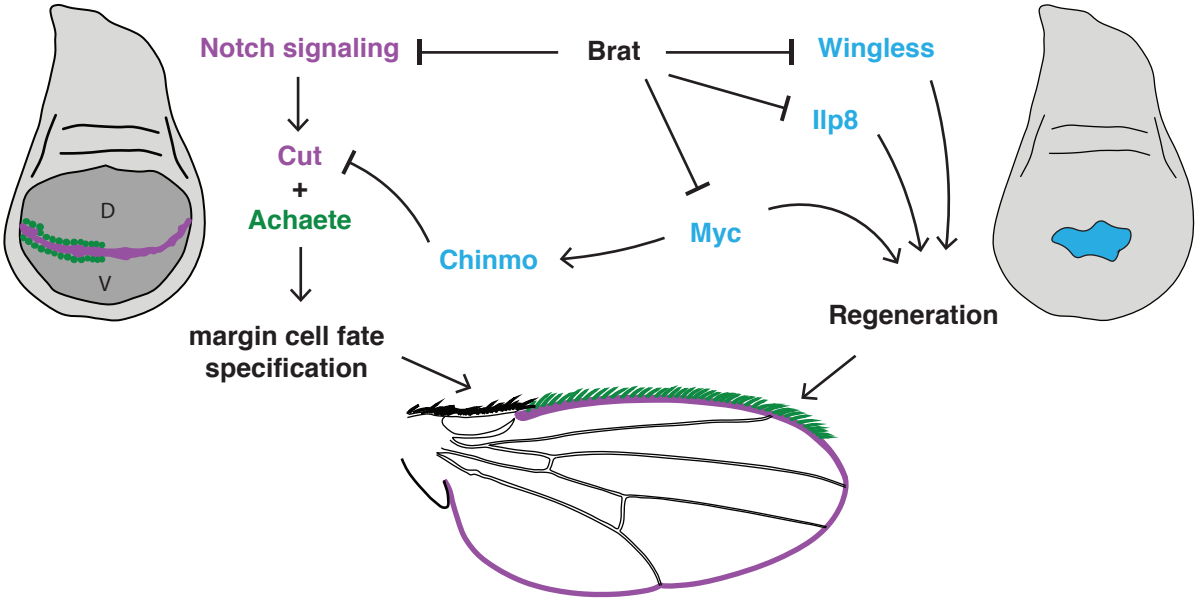
Notch signaling
Brat
Wingless
Ilp8
Cut
+
Achaete
Chinmo
Myc
D
V
margin cell fate
specification
Regeneration

Fig 8. Brat restricts pro-regeneration factors and ensures correct margin cell-fate specification.

Model describing the network of Brat targets in the regenerating wing imaginal disc. Importantly, Brat restricts Myc levels, limiting expression of Myc's targets, including Chinmo, to allow correct margin cell-fate specification.